(4)

A TRIDENT SCHOLAR PROJECT REPORT

NO. 173

" A Model of the Acoustic Interactions Occurring Under Arctic Ice "

UNITED STATES NAVAL ACADEMY
ANNAPOLIS, MARYLAND

UNCLASSIFIED

SECURITY CLASSIFICATION OF THIS PAGE *(When Data Entered)*

REPORT DOCUMENTATION PAGE		READ INSTRUCTIONS BEFORE COMPLETING FORM
1. REPORT NUMBER U.S.N.A. - TSPR; 173 (1990)	2. GOVT ACCESSION NO.	3. RECIPIENT'S CATALOG NUMBER
4. TITLE *(and Subtitle)* A MODEL OF THE ACOUSTIC INTERACTIONS OCCURRING UNDER ARCTIC ICE.		5. TYPE OF REPORT & PERIOD COVERED Final 1989/90 6. PERFORMING ORG. REPORT NUMBER
7. AUTHOR(s) Roger R. Ullman, II		8. CONTRACT OR GRANT NUMBER(s)
9. PERFORMING ORGANIZATION NAME AND ADDRESS United States Naval Academy, Annapolis.		10. PROGRAM ELEMENT, PROJECT, TASK AREA & WORK UNIT NUMBERS
11. CONTROLLING OFFICE NAME AND ADDRESS United States Naval Academy, Annapolis.		12. REPORT DATE 22 May 1990 13. NUMBER OF PAGES 105
14. MONITORING AGENCY NAME & ADDRESS *(if different from Controlling Office)*		15. SECURITY CLASS *(of this report)* 15a. DECLASSIFICATION/DOWNGRADING SCHEDULE

16. DISTRIBUTION STATEMENT *(of this Report)*

This document has been approved for public release; its distribution is UNLIMITED.

17. DISTRIBUTION STATEMENT *(of the abstract entered in Block 20, if different from Report)*

18. SUPPLEMENTARY NOTES

Accepted by the U.S. Trident Scholar Committee.

19. KEY WORDS *(Continue on reverse side if necessary and identify by block number)*

Underwater acoustics
Sea ice - Arctic regions

20. ABSTRACT *(Continue on reverse side if necessary and identify by block number)*

Underwater sound interacting with the Arctic ice cover is reflected from the plane surface as well as scattered due to small-scale roughness elements and large pressure-ridge keel structures. Experiments modeled the acoustic-ice interactions using burst transmissions from omnidirectional underwater point sources. Floating acrylic plates were employed to represent the Arctic ice due to similarity in impedance →

(OVER)

DD FORM 1 JAN 73 1473 EDITION OF 1 NOV 65 IS OBSOLETE
S/N 0102-LF-014-6601

UNCLASSIFIED

SECURITY CLASSIFICATION OF THIS PAGE *(When Data Entered)*

characteristics and other physical properties to known ice values. Geometrical properties of the ice were accurately scaled in the acrylic by maintaining the appropriate wavelength ratios. Reflection and forwardscatter effects were analyzed and compared with existing theories for the Arctic.

U.S.N.A. - Trident Scholar project report; no. 173 (1990)

" A Model of the Acoustic Interactions Occurring Under Arctic Ice "

A Trident Scholar Project Report

by

Midshipman Roger R. Ullman, II, Class of 1990

U.S. Naval Academy

Annapolis, Maryland

Leonyx G. Baker

LCDR Leonyx G. Baker - Oceanography Department

Accepted for Trident Scholar Committee

Dennis T. Hasson

Chairperson

22 May 1990

Date

ABSTRACT

Underwater sound interacting with the Arctic ice cover is reflected from the plane surface as well as scattered due to small-scale roughness elements and large pressure-ridge keel structures. Experiments modeled the acoustic-ice interactions using burst transmissions from omnidirectional underwater point sources. Floating acrylic plates were employed to represent the Arctic ice due to similarity in impedance characteristics and other physical properties to known ice values. Geometrical properties of the ice were accurately scaled in the acrylic by maintaining the appropriate wavelength ratios. Reflection and forwardscatter effects were analyzed and compared with existing theories for the Arctic.

ACKNOWLEDGMENTS

I am sincerely indebted to the following people:

Midshipman First Class Mark Watkins for his patient work explaining the mysteries of TK Solver to a true computer illiterate.

The U.S. Naval Academy Math Department for helping me explore the bounds of complex trigonometry.

Mrs. Rachel Heberle, without whose help and artistic influence I could never have completed my poster successfully.

Mr. Bobby Bates and Mr. Clarence Woods of the Math and Science Department for their superb workmanship in crafting the acrylic keels used in this experiment.

My parents, Mr. and Mrs. Roger Ullman, for their support despite not really knowing what I was doing, its relevance to the real world, or why I would chose to dig myself so deep a hole in my First Class year.

Midshipman First Class Matthew Simms for keeping me awake through many late night work sessions and inspiring me to

achieve through the example of his own hard work for our four years together by the Bay.

CDR M. P. Cavanaugh for subtly convincing me, without my knowledge, that I really wanted to accept the challenge of being a Trident Scholar.

Finally and without a doubt, most importantly, my advisor, LCDR Leonyx G. Baker, for his unending support throughout the entire project. His ability to excite my academic interest and to discover perpetually the positive side, whether it be a temporary setback in the laboratory or an impasse in theoretical computations, is what carried me to completion of this project and allowed me to graduate on time.

TABLE OF CONTENTS

LIST OF TABLES

LIST OF FIGURES

I. INTRODUCTION

Recent advances in the under-ice capabilities of the Soviet naval forces include the ability to fire through ice cover as noted by Covault (1984). LANDSAT images of 28 March 1984 indicate broken ice caused by Soviet submarine operations. When linked with the desire for increased exploration of fossil fuel deposits and the determination of oil spill locations (Francois and Wen, 1983), reasons for renewed interest in Arctic acoustics become apparent. This unique Arctic environment presents a multitude of questions which are central to the study of sound propagation, as well as a virtually noise-free environment in which to seek to resolve them. Current naval developments, relevant to both sonar operations and underwater weapons performance, and technological advances, enabling industry to access previously unattainable natural resources, have simply highlighted the importance of study in this region.

The experiments conducted in this study modeled the acoustic energy-ice interactions using acrylic to represent the Arctic ice. This substance was chosen due to its similiarity in impedance characteristics and other physical properties to known ice values.

Plane models simulating the large expanses of relatively flat pack ice, as well as keel models to

explore the interactions in the regions of pressure-ridges, were employed. Reflection and forwardscatter effects were analyzed as these account for the majority of the energy in the Arctic acoustic budget and directly affect long-range sound propagation.

A detailed investigation of the Arctic environment provided the background for selecting an appropriate representational forum. Experimental data were then compared to existing theories for the Arctic, demonstrating the relative merits of a variety of equational modeling techniques.

II. ACOUSTIC PERSPECTIVE OF THE ENVIRONMENT

A. OPEN OCEAN ACOUSTIC ENVIRONMENT

Any study of Arctic acoustics inherently requires a knowledge of typical open ocean sound propagation phenomena. As acoustic energy propagates through a medium it generates a density disturbance. The compressions and rarefactions of the waves manifest themselves as increases and decreases of the point densities along the path of travel. Thus, the velocity (or celerity) of wave propagation is a function of the density of the medium; in the case of acoustic waves in the ocean, this medium is sea water.

The density of sea water is a function of temperature, salinity, and pressure; these three factors determine the propagation characteristics as well. Pressure increases linearly with depth, and the salinity for any finite region of the open ocean can be assumed to be roughly constant both vertically and horizontally. Therefore, the dictating factor for sound speed determinations in the "upper" or "operational" regions (anything less than 1000 meters) becomes temperature.

The ocean's upper region is, in fact, composed of several layers of differing temperature gradients, each of which is prone to variation due to daily, seasonal, and biological effects. At depths greater than 1000 meters

the temperature gradient decreases markedly as the water temperature converges to a constant four degrees Centigrade (°C). This temperature profile causes a relatively constant, pressure-driven, positive sound speed gradient underlying the volatile upper layers which, in general, demonstrate a negative gradient. A common open-ocean sound velocity profile, (a depiction of celerity versus depth), is shown in Figure 1. The resulting propagation pattern is demonstrated by Figure 2 and exhibits an environmentally created waveguide or sound channel. This is caused by the natural tendency of sound to refract toward regions of slower sound velocity.

Attenuation of acoustic waves is affected by molecular relaxations of magnesium sulfate, boric acid, and magnesium carbonate present in the water (Mellen, 1987). These effects are frequency dependent with higher frequencies being more severely attenuated than lower ones. Additionally, interactions with the water/air interface and the sea floor account for losses as a portion of the energy is transmitted into the adjacent media.

B. THE UNIQUE ARCTIC ENVIRONMENT

Acoustic wave propagation and scattering in the Arctic pose several problems supplemental to those of the typical open-ocean environment. The existence of unique hydrothermal conditions is one factor. The surface layer

Typical Open-ocean Sound Velocity Profile

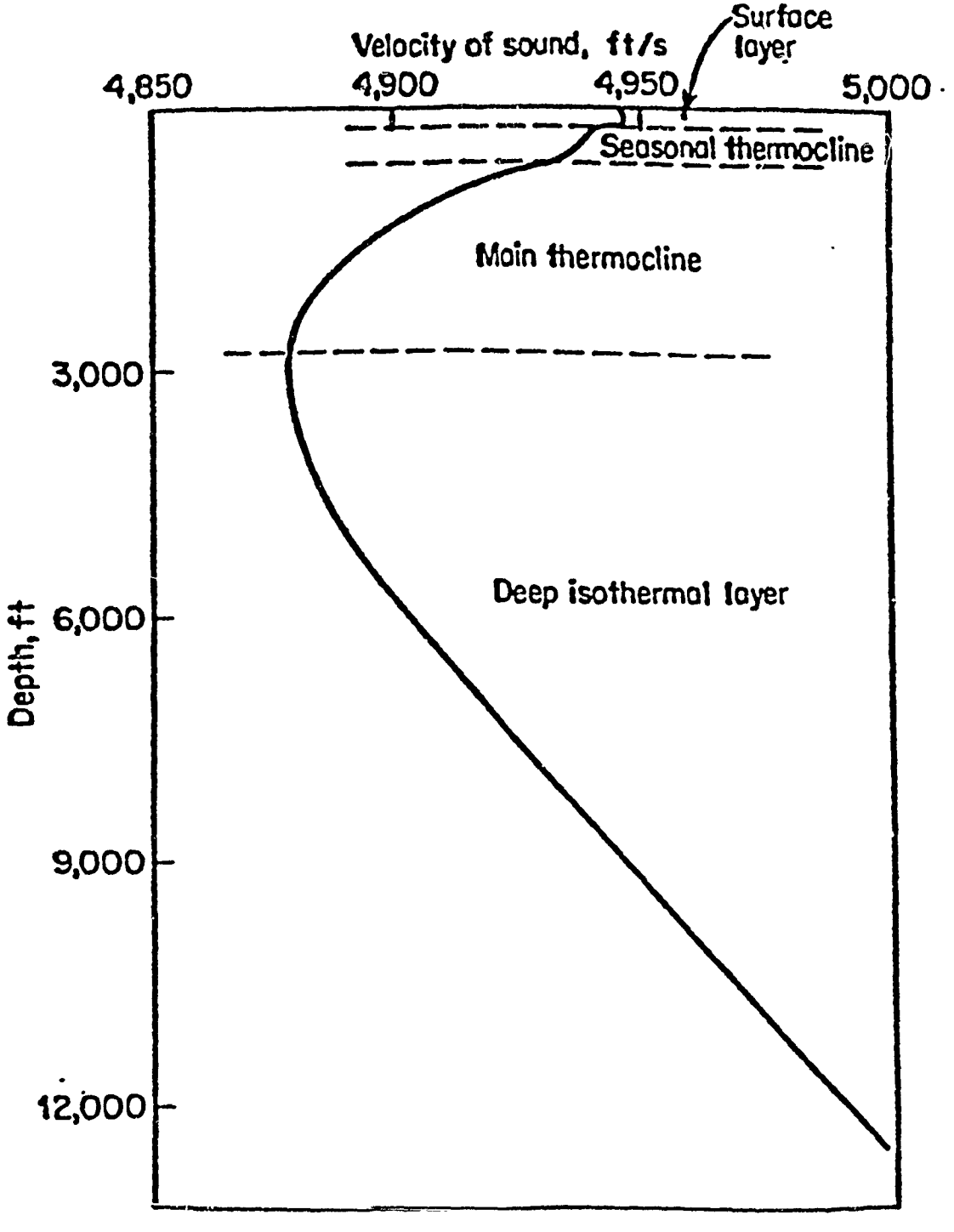

Figure 1. A typical open ocean sound velocity profile. (Urick, 1983)

Open-Ocean Propagation Paths

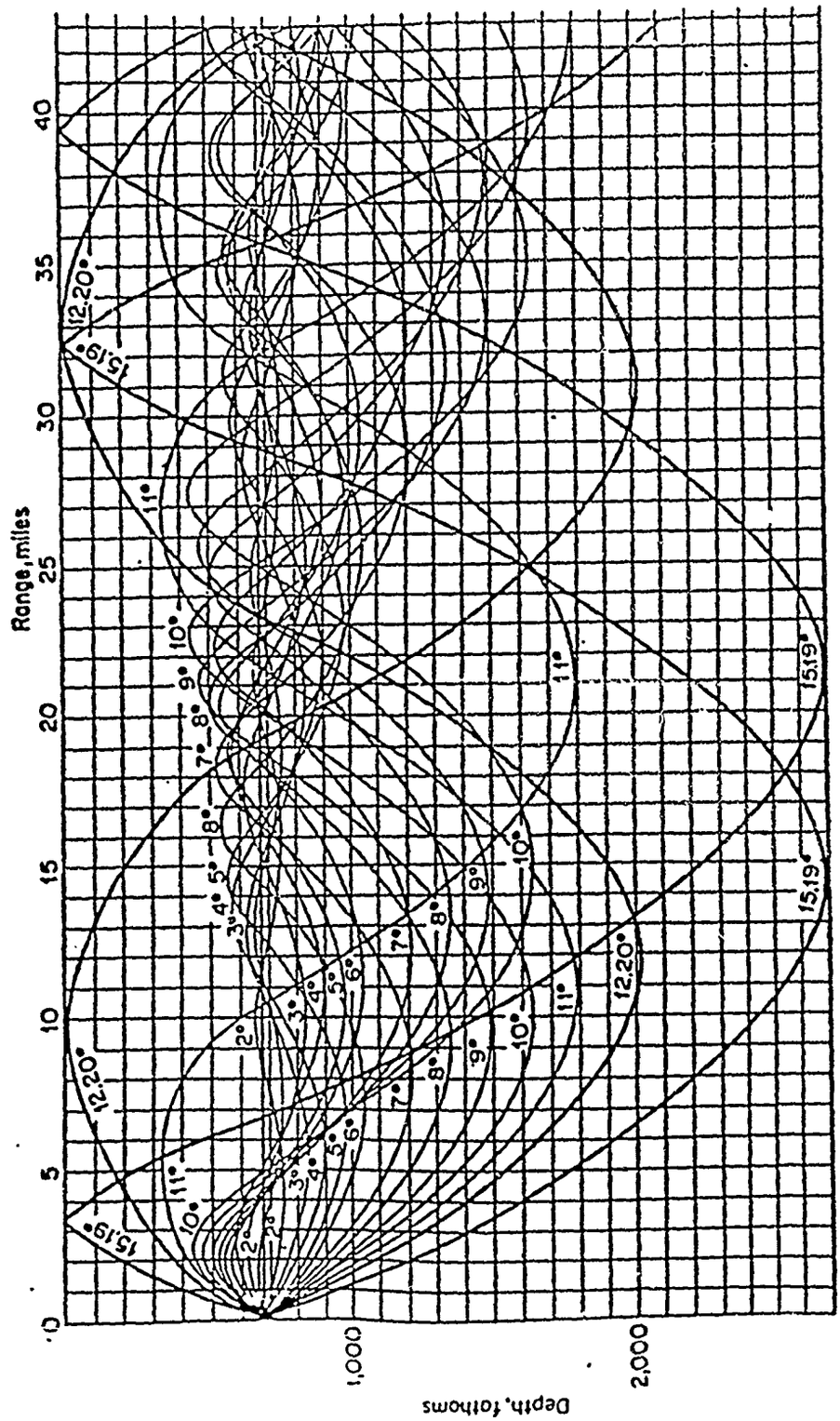

Figure 2. A depiction of typical open ocean propagation paths. (Urick, 1983)

is at or near the freezing point, which for fresh water is 0° C and for sea water is -2° C. Additionally the layer salinity is dilute, with values between 28 and 32 parts per thousand (ppt), relative to a 34.7 ppt average in the open ocean. This is due to the process by which the ice precipitates salts after freezing. Below 50 meters, however, a sharp salinity increase with depth is noted.

The next layer is termed the "Atlantic layer" and ranges from 150 to 900 m. Temperatures above 0° C and as great as 3° C may exist in this region. It is further characterized by a relatively uniform salinity. The combination of these factors with pressure effects results in a monotonic increase with depth of density, and thus acoustic speed, in this layer.

The bottom region, which may extend to depths of 4846 m as in the Greenland Sea (Welsh et al., 1986), demonstrates a highly uniform salinity, with values between 34.93 and 34.99 ppt and a uniform temperature of 0 °C. Density in this layer becomes a function of pressure. Figure 3 depicts the variation of the salinity and temperature parameters with depth in the Arctic. Figure 4 demonstrates the resulting typical sound velocity profile.

Upward path refraction and, therefore, repeated interaction with the overlying pack ice, results from sound's propensity to travel toward regions of slower

Arctic Temperature and Salinity Profiles

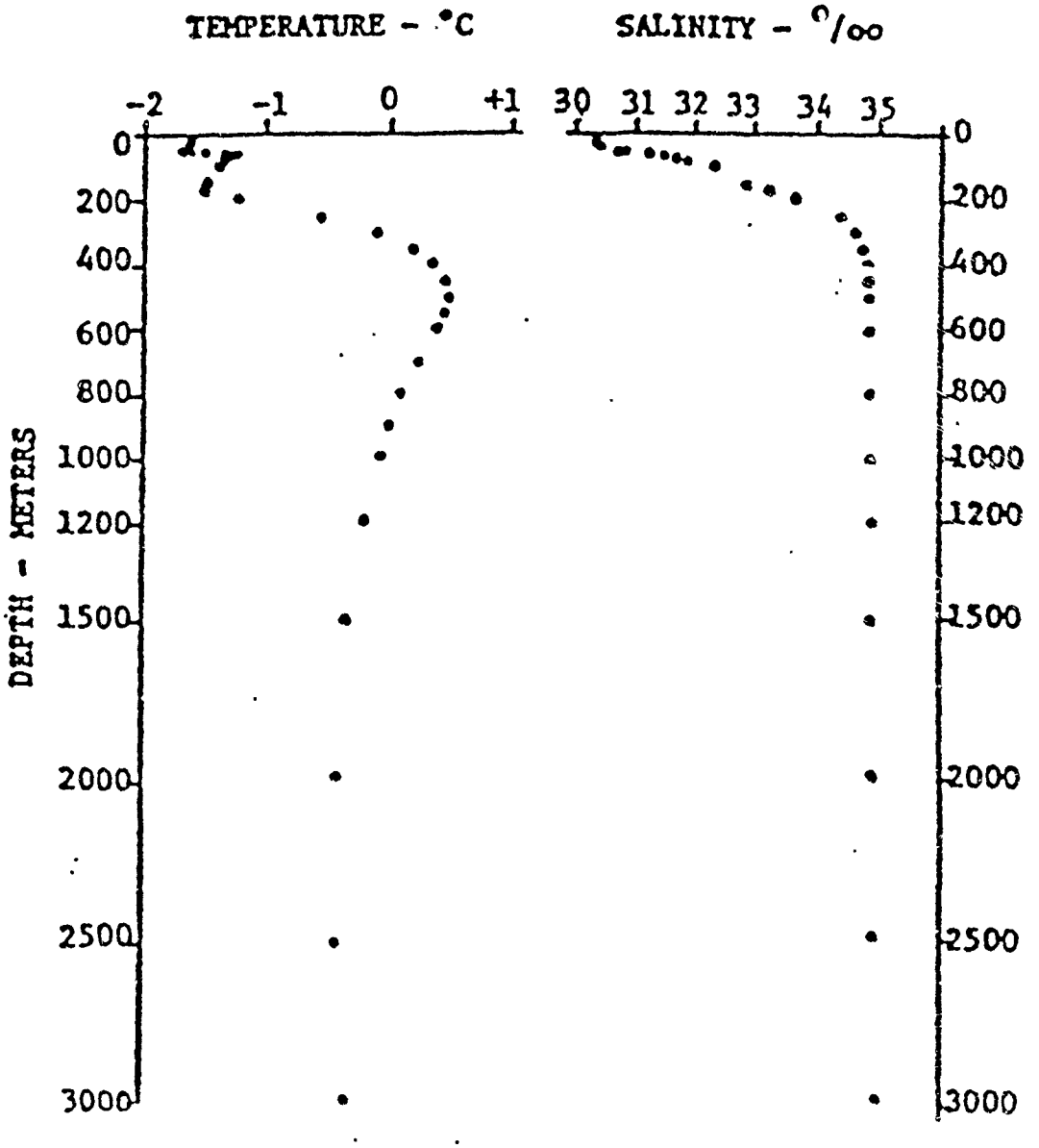

Figure 3. Temperature and salinity profiles typical of the Arctic environment (Urick, 1983)

Typical Arctic Sound Velocity Profile

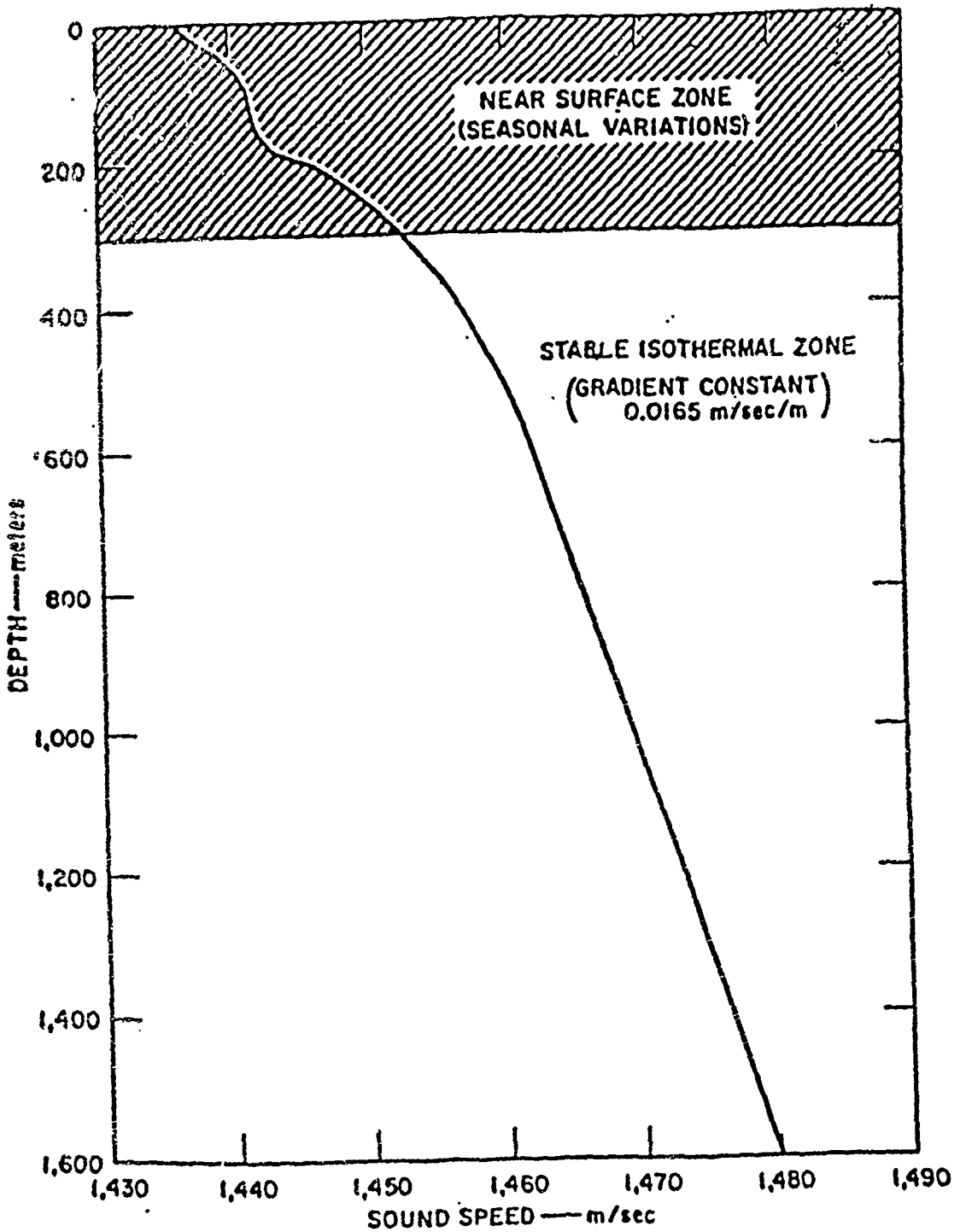

Figure 4. A typical Arctic sound velocity profile. (Urick, 1983)

celerity. In the profile commonly found in the Arctic, where sound speed increases monotonically with depth, this propagation pattern is known as "half-channel ducting", as it demonstrates only the lower half of the propagation pattern found in typical deep sound channels in the open ocean (Figure 5). It is important to note the difference in scales of the two axes in Figure 5; these refractive effects occur over long horizontal distances, and the waves do not come in contact with the surface as frequently as might initially appear.

Long-range propagation paths which intersect the sea floor essentially do not exist; thus, sea floor interaction is a negligible cause of loss. Repeated sound wave interaction with the surface is therefore responsible for the majority of the losses incurred in the Arctic acoustic energy budget. The existence of a liquid/solid boundary at the surface results in an increase in observed losses over values found in non-polar regions where the junction is liquid/gas. At the sea water/air interface, the reflection coefficient is nearly unity due to the large disparity between the acoustic impedances of the two substances, water and air. In the Arctic, however, variations in the ice composition and incident angle of the waves can result in values of the surface pressure reflection coefficient ranging from -1 to 1. Understanding the interactions that occur at the junction of the two

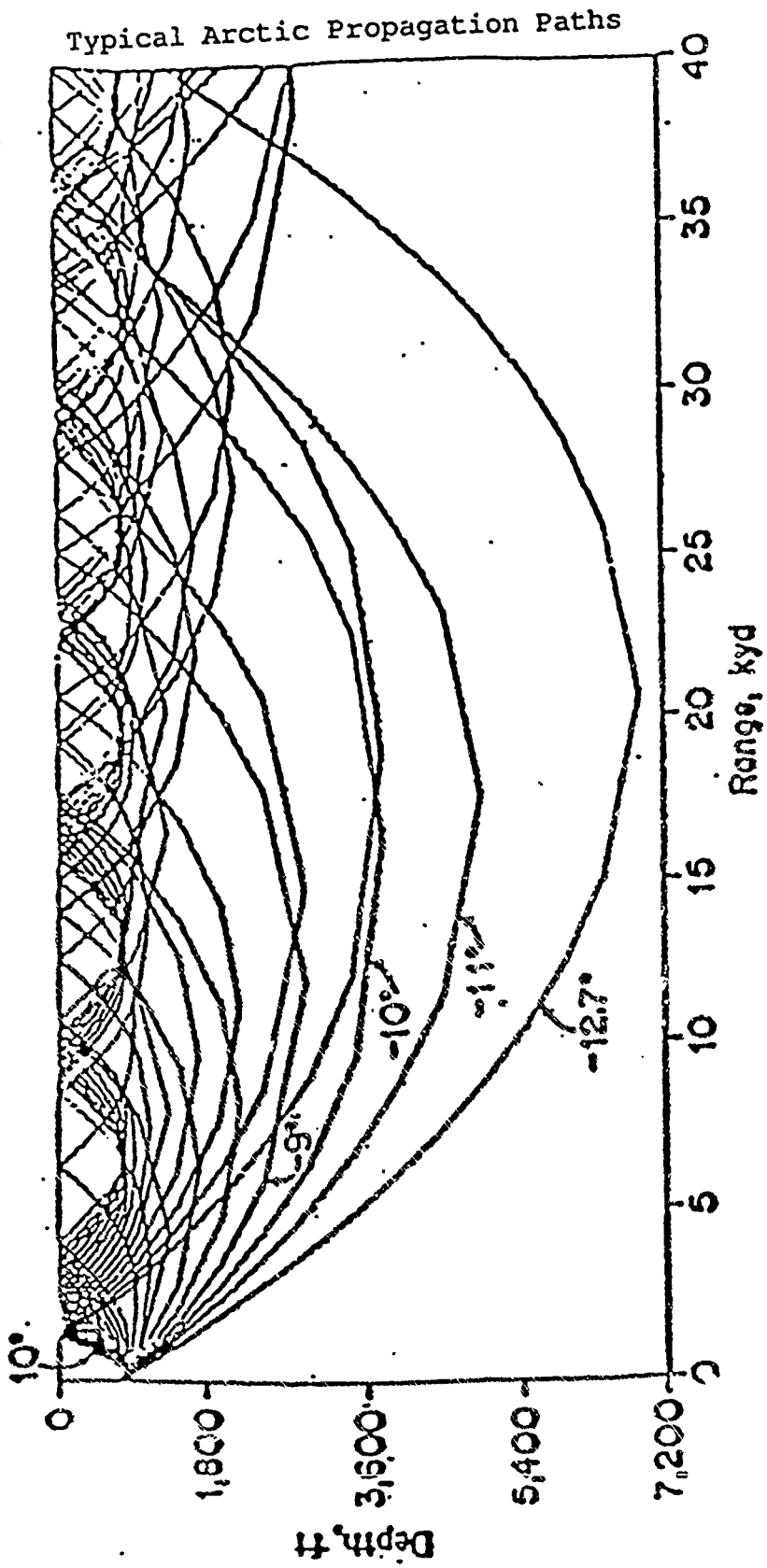

Figure 5. A depiction of typical Arctic propagation paths. (Diachok, 1974)

media and in the ice thus becomes crucial. This is particularly true at the lower frequencies where attenuation due to chemical effects does not play as key a role and long distance propagation is possible.

Ice is a solid and can therefore support both compressional and shear waves. This accounts for a great deal of the increase in observed surface losses. However, ice is both inhomogeneous in composition and not fully of the solid phase; it is a lossy (a substance causing attenuation or dissipation) multi-layered viscoelastic medium, adding further complexity. A precise deterministic equation for the amount of energy absorbed by the ice, what portion of the incident pressure returns as a reflected wave, and how much energy is reradiated later into the water does not yet exist (Browne, 1987). Although extensive probablistic equations do exist for the reflection at a liquid-solid interface where the solid is upper-bounded by air, the lack of specific data concerning the inhomogeneous ice composition and surface structure precludes derivation of such an equation. Until a method for determining this equation is found, an understanding of reflection interaction at the interface will be incomplete.

C. ICE CHARACTERISTICS

1. ICE FORMATION

Sea ice begins to form on the surface when the water temperature is below the freezing point of -2° C. Initially, minute spheres develop, forming individual ice discs or platelets of 2 to 3 millimeters (mm) diameter. Growth perpendicular to the principal hexagonal axis is most rapid, thus the ice forms with this axis vertical (Welsh, 1986). The orientation of the newly formed discs is subsequently altered by water motion. Collisions with other crystals ensure that they remain reasonably well-rounded; fusion occurs when the platelets are brought into contact with each other under pressure.

Although all of the discs begin to form in a similar structural manner, the turbulent collisions to which they are subjected result in mutation and realignment of the initial axes of formation. Thus from the outset, the newly forming ice cover is composed of a randomly oriented crystalline structure. These weakly bound ice crystals are termed "new" ice and may include "frazil" ice, "grease" ice, "slush" and "shuga". They typically exhibit a salinity greater than 5 ppt (Welsh 1986).

As this inital layer begins solidification, further ice growth occurs on the bottom. The congealing ice is now at least a few centimeters in thickness and is termed

"nilas" until it reaches 10 cm. Separation of individual brine salts begins to occur due to gravity and temperature effects at this point in the ice development. The resulting mass of sea ice is vertically and horizontally stratified and inundated with deposits of salts and air, in addition to the chemicals that exist already within the ice lattice structure (Vidmar, 1987).

The "young" ice stage follows and is composed of ice from 10 to 30 cm. "First year" ice by definiton is any ice that has developed in one growth season and may be anywhere from 30 cm to 2 m in thickness. Preferential ice crystal formation may exist at this stage based upon under-ice current flow.

"Old", "multi-year" or "level" ice is defined as ice that has survived one summer's melt season. It may be thinner than two meters or as thick as five meters. Ice in this final developmental stage contributes to pressure-ridge structures (sails and keels). The depth of such a keel is a function of the ice thickness. Multi-year ice may be distinguished from first-year ice as it is more rounded and generally thicker.

As brine freezes within the ice, it becomes concentrated in small pockets, the majority of which have been observed to be spheroidal (Bunney, 1974). These spheres of increased salinity sea water (brine) may serve as additional acoustic scattering centers. Regardless,

they disrupt the acoustic propagation by altering the properties of the medium. What initially appears a rather simple substance is highly inhomogeneous from the outset. Variation in crystalline orientation, ice composition, salt concentrations, and thickness all exist in the micro-scale, resulting in a complicated, depth dependent, anisotropic medium (Vidmar, 1987).

Icebergs are massive segments of fresh water ice that have broken off or "calved" from the terminus of a glacier or ice shelf. They may be distinguished by their size, high relief, large freeboard and irregular shape. They are present primarily in the Marginal Ice Zone (MIZ) and are thus not of particular importance to the Arctic acoustician.

2. CHEMICAL AND COMPOSITIONAL TRANSFORMATIONS

As time elapses, the effects of gravity and temperature begin to be evident, and the newly formed ice cover commences salt precipitation. Ice that formed more quickly entrapped a higher concentration of the various salts existing in the generating water, whereas slower forming ice is of a lower salinity. Salt excretion causes the surface water layer to increase in density and thereby initiates mixing. This accounts for the nearly constant salinity at depth with a particularly dilute overlying surface layer.

Ice may also form on the sea floor. This is referred to as "anchor ice". The buoyancy produced by the transition into the solid phase results in ascension of the newly formed ice. Once it floats to the base of the surface ice, it becomes frozen in place and incorporated into the overlying Arctic cover. Sea floor sediments and biological specimens thereby become consolidated within the increasingly anisotropic surface ice layer (Klieinerman, 1980).

3. PHYSICAL TRANSFORMATIONS

Not only is the ice inhomogeneous in composition and structure, but it is not static. Movements of the entire ice sheet are caused by winds, currents, waves and swell. Gravity effects and temperature changes can cause cracking of the surface. These movements further reorient the internal air or brine structures and individual ice crystals, adding to the inhomogeneity of acoustic property distribution.

Numerous structures on the surface are created as a result of movement, as the sheets break or crack and subsequently override one another while being forced together. Sails or "hummocks" form above the ice layer and keels or "bummocks" below the surface. Ice movement may be likened to the plate tectonic motion of the earth's crust, for the edges of two ice sheets interact in a very

similar manner. Sail formation would be likened to mountain development in this analogy. The difference between the two processes is the lack of dissolution of the supressed or subducted layer; the ice simply forms a keel.

These pressure-ridge keels provide a large population and a data base for detailed study regarding size, spacing and frequency of occurrence. They are thus of great interest to statisticians. Hibler et al. (1974), utilizing visual measurements above the ice and submarine underice profiles, developed a statistical model of pressure ridge keel depths and spatial density. A threshhold on the depth of structures that would be large enough to be considered in the distribution was chosen, ensuring that only veritable keels would be evaluated in the data and that minute roughness elements would not alter the sample population. The average depth for all keels in the population below the cutoff depth of 6.1 m was 9.6 m with an average width of 36.2 m and a median distribution of 4.3 keels per km (Hibler et al., 1974).

Floe collision forms fields of random ice rubble in addition to the more simple vertical ridge structures. Further complexity is caused by gaps that develop in the ice sheet. "Leads" are cracks in the ice resembling rivers. "Polynya" is the term denoting large holes resembling lakes. These expansion formations add multiple

edge surfaces and combine with the already present surface roughness factors to cause a highly complex acoustic environment. Finally, a varying snow cover adds an additional layer of unique acoustic properties and thereby further complicates analyses.

D. DIFFICULTY OF STUDY

The Arctic environment presents a broad range of parameters to the acoustician and a plethora of variables not present in the open ocean. It has thus been a region of intense study, an example of which is the multiple MIZEX (Marginal Ice Zone Experiments). There are, however, numerous difficulties encountered when seeking to study the Arctic. The primary and most obvious limitation to scientific research is the Arctic environment itself. Severe weather patterns as well as the extremes in temperature experienced there make the development of any *in situ* measurements particularly difficult both from the standpoint of human and equipment factors (Welsh, 1986). Its remote location and harsh climate render study extremely difficult.

Despite these obstacles, the region under the pack ice of the Arctic is one of the quietest acoustically, due to the lack of sea state, biological, and shipping effects that all contribute to ambient noise in non-polar regions. Further, high frequency noise is quickly attenuated due to the scattering effects of the rough under-ice surface.

The more easily accessible Marginal or Seasonal Sea Ice Zone (MIZ or SSIZ) is, however, among the noisiest regions on the planet acoustically. All of the typical contributing factors to ambient noise exist here with several additions. Cracking and buckling ice, wave-ice floe interaction and noise caused by the movements and collisions of the ice all add to the cacophony.

Scattering due to submerged ice keels clutters the environment further. Surface ice sails and submerged keels alter the ice thickness; the geometric and thus acoustic properties of the ice change. Minute surface roughness factors of Arctic sheet ice contribute to the complexity of the environment and to scattering. Losses may also result from an air layer trapped between the sea and the ice cap.

A zone of "partial freezing" up to 20 centimeters thick in which the sea water has properties of both solid and liquid is another region of attenuation. The acoustic chain of events that occurs between the solid ice sheet and the underlying liquid sea water in this "fluid" or

"colloidal" region has yet to be fully explained (Bunney, 1974). This region of partial freezing lends itself well to a multitude of questions regarding its structure, formation, resulting effects on the acoustic environment, etc.

Finally, the transportation of ice samples, which would alleviate some of the environmental difficulties, has proven to be rather infeasable and the subsequent test results somewhat inaccurate due to the chemical changes that occur as the ice is subjected to temperature and gravity variations. Drainage of brine during "coring" (or collection) of the ice samples and surface melting during experimentation alter the properties, as well, rendering transportation rather inutile (Vidmar, 1987).

A numerical model for the acoustic reflection in the Arctic region, particularly at "lower" frequencies (less than one kilohertz), where present model results tend to diverge from the environmentally derived data, may help obtain a more complete understanding of sound propagation (Mellen, 1987). Additionally, the development of a model for prediction of the ice sheet's characteristics, depth, and acoustic properties based on easily discernible factors such as temperature, salinity and pressure is sought. This will lead to a more complete acoustic model of the Arctic region throughout all frequency ranges.

A detailed understanding of the phase change of sea water may present new insights into the sound patterns observed in the colloidal region. Likewise, the propagation of acoustic waves through the ice, either as compressional or shear waves, provides another avenue for attenuated energy and deserves attention. Reradiation from the solid supplements scattering and signal interference. There are thus a myriad of additional variables with which the acoustician must be concerned when working in the Arctic environment additional to those of import in the open ocean basins.

III. EXPERIMENTAL PROCEDURE

Ice was modeled using acrylic plate in an effort to explore the interactions that occur under the Arctic pack and thereby gain further insight into long-range propagation phenomena. These scale models were floated in two large tanks and impinged upon by burst emissions of six different frequencies. Reflection and forwardscatter data were then collected.

A. EQUIPMENT EMPLOYED

Two different tanks provided the environment for this experiment. The first was a 353.3 liter (L) tank with dimensions of: length - 180.5 cm, width - 43.5 cm, depth - 45 cm. The second tank employed had a volume of 11.6 kL and dimensions of: length - 3.2 m, width - 2.8 m, depth - 2.3 m. The use of two different sized tanks expanded the range of angles that were geometrically feasible, thereby enlarging the final data base.

Neither tank was anechoic or acoustically isolated. The smaller tank was subject to 60 Hz signals from nearby laboratory equipment which added undesired noise to the environment. The larger tank exhibited far more ambient clutter. This 11.6 kL tank, bolted to the foundation and connected to a series of pumps and motors, is acoustically coupled to a plethora of noise sources. Although this

ambient noise should have had little bearing on the data, as the frequencies with which the experiment was concerned were a minimum of three orders of magnitude larger, it is important to note that this noise did exist.

A filter was not used to remove this low frequency noise, since burst or pulse emission was employed in the model. A burst is formed from a sum of frequencies as per the Fourier theorem; removing any of the lower frequency components would have altered the received pulse.

Figure 6 illustrates the equipment organization employed for the experiments. Equipment utilized is listed in Table I. A more detailed explanation of specific equipment capability and usage proceeds below.

1. Wavetek 20 MHz Function Generator Model 191

The Wavetek function generator operates in a frequency range of .002 Hz to 20 MHz. It is capable of sine, triangle, and square wave output ranging from 1.5 millivolts peak to peak (mV_{p-p}) to 30 V_{p-p}. It supplies a peak current of 150 milliamps that may be continuously varied over an 80 deciBel (dB) range.

The function generator served as the source of the acoustic energy and was primarily employed in the double pulse mode. This mode emits a signal of two complete cycles at a given frequency when the trigger is activated; this will be termed a pulse or burst. The manual trigger

Equipment Configuration

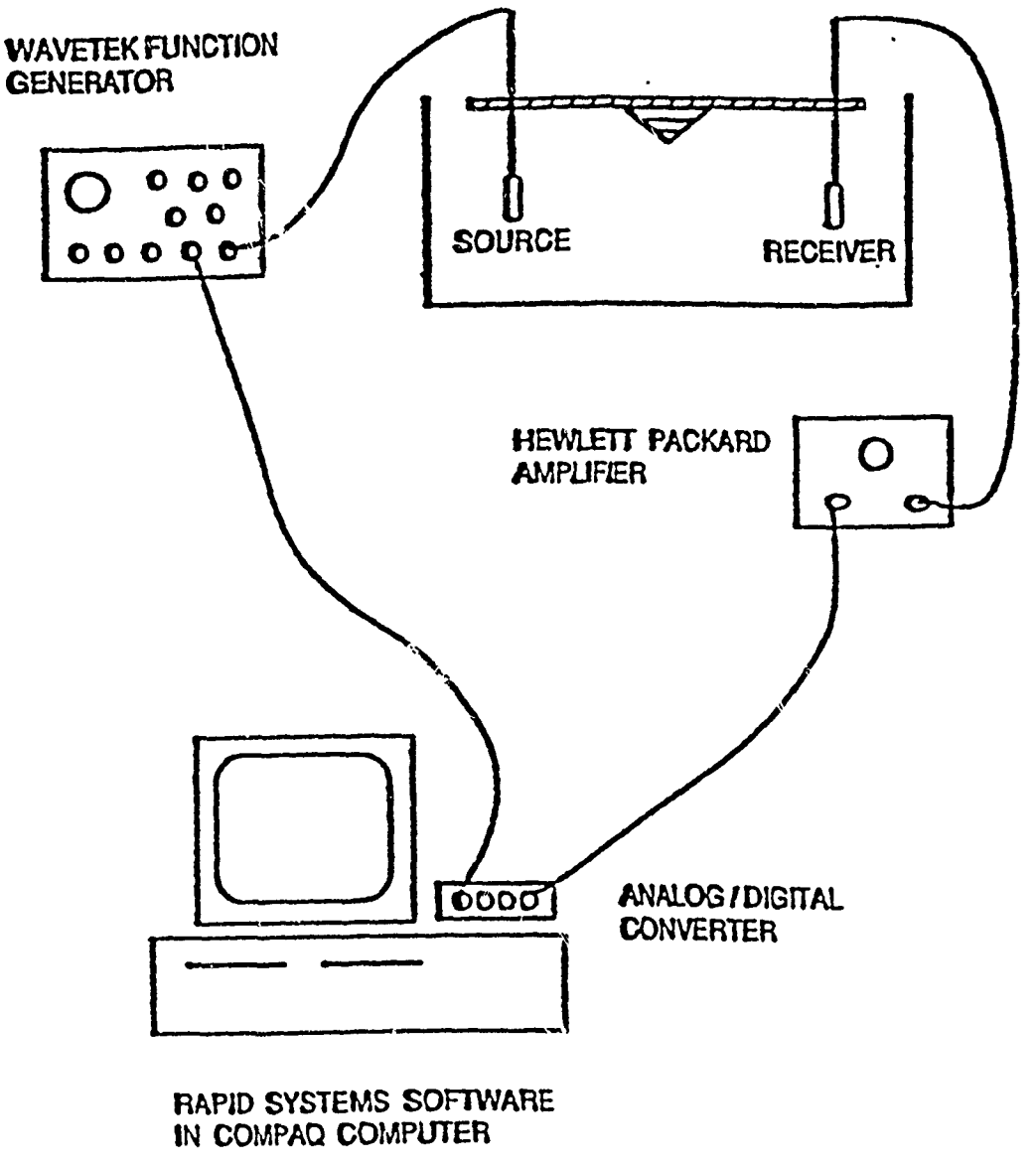

Figure 6. Equipment configuration for the experiments

TABLE I

EQUIPMENT LIST

Abbreviation	Nomenclature
Amplifier	Hewlett Packard AC Amplifier, Model 466A
Source or Receiver	Celesco LC-10 Hydrophone
Function Generator	Wavetek 20 MHz Function Generator, Model 191
Spectrum Analyzer	Rapid Systems Real Time Spectrum Analyzer, Model R360 with Data Acquisition and Analysis Package
Computer/Oscilloscope	Compaq DESKPRO computer and Amdek Color 600 monitor
Analog/Digital Converter	Rapid Systems 4X4 Digital Oscilloscope peripheral analog/digital converter

configuration was utilized which permitted the operator to control the frequency of pulse propagation and allow adequate time between emitted signals for echoes in the tank to dissipate.

2. Celesco LC-10 Hydrophones

Two Celesco LC-10 Hydrophones were used as omni-directional source and receiver in the laboratory. Their lightweight highly portable nature facilitated adjustments within the tank. The 40 cm of connection cord immediately adjacent to the hydrophones was encased within a plastic tube and marked with centimeter gradations to ensure proper hydrophone depth, orientation, and stability once placed.

3. Hewlett Packard AC Amplifier Model 466A

A Hewlett Packard AC Amplifier was employed to enhance the return signal from the receiving hydrophone before being routed for processing into the Real Time Analyzer. It is capable of 0, 20 and 40 dB signal gain and was utilized in the 40 dB gain configuration primarily.

4. Rapid Systems Real Time Spectrum Analyzer Model R360

The Rapid Systems Real Time Spectrum Analyzer with the 4X4 Digital Oscilloscope peripheral, R300 Digital Signal Processing Interface Board, and R360 Real Time Spectrum Analyzer software was installed in the Compaq DESKPRO

computer. It provided the heart of the signal acquisition and analyzation. The frequency spectrum capabilities permitted calibration of the function generator frequency accuracy. The saving mode allowed the pulses to be recorded onto 5-¼" floppy disks for later examination. Analysis techniques are described in the following section.

The software package enables [illegible] time and voltage readings of the wave signals. Sampling and display time can be altered, essentially compressing or expanding the waveform information. The 40 microsecond (μsec) mode (the smallest sampling interval) was used throughout. Several trigger options are available; however, only the digital mode was used in this experiment. The digital configuration begins collection of the 2048 data points at 0 volts and the first indication of a positive slope (i.e. as soon as the emitted pulse was triggered). A viewtime delay may be entered; this option was not chosen in order to allow the operator to view the emitted and reflected pulses immediately. Gain of the channels can be individually manipulated to facilitate viewing, and there are various options for summing the channel displays. The variable pulse or "non-summing" option was chosen, as this permitted separation and independent viewing of the source pulse from those received.

5. Compaq DESKPRO computer and Amdek Color 600 monitor

The Compaq computer housed the Rapid Systems software. The Color 600 monitor served fundamentally as the oscilloscope in this configuration and enabled viewing of the data collection.

B. DESCRIPTION OF PHYSICAL MODELS

Acrylic was chosen as the medium for the model due to its similarity to the known parameters of Arctic ice. Table II presents a comparison of values for the acrylic employed in the laboratory and those reported in the literature for typical Arctic ice.

The compressional wave speed (c_{p2}), acoustic impedance ($\rho_2 c_{p2}$) and bulk modulus (E) of the acrylic all lie centrally within the range of typical Arctic values. The density of the acrylic (ρ_2) is approximately 25% too high and the shear wave speed (c_{s2}) is roughly 10% too low. The rigidity or shear modulus (G) is low by a factor of three, but the remainder of the parameters of the acrylic show good agreement with the ice values when scaled for the appropriate wavelengths. Medwin et al. (1988), Denny and Johnson (1986) and Browne (1987) have previously demonstrated the effectiveness of acrylic as a modeling medium for Arctic ice.

TABLE II

COMPARISON OF ARCTIC, EXPERIMENTAL AND THEORETICAL VALUES

Parameter	Arctic Values		Laboratory Model Value	Model/Arctic Ratio
	Range	Typical		
1. Density of Water ρ_1 (kg/m^3)	1000-1040[a]	1026[a]	998.035[b]	.9596 - .9980
2. Density of Ice ρ_2 (kg/m^3)	760-960[c]	910[c]	1180[d] 1189.8[b]	1.229 - 1.553 1.239 - 1.566
3. Compressional Wave Speed of Water c_{p1} (m/s)	1440-1485[e]	1440[e]	1500[d]	1.042 - 1.010
4. Compressional Wave Speed of Ice c_{p2} (m/s)	2100-3800[f]	3375[f]	2201.09[d] 1939.03[b]	.5792 - 1.049 .5103 - .9233
5. Shear Wave Speed of Ice c_{s2} (m/s)	1100-1900[f]	1650[f]	1029.503[d] 931.5[b]	.5418 - .9359 .4903 - .8468
6. Acoustic Impedance of Water Z_{H2O} (10^6 Rayls)	1.44-1.544[g]	1.477[g]	1.497[g]	.9696 - 1.040
7. Acoustic Impedance of Ice Z_{ice} (10^6 Rayls)	1.596-3.648[g]	3.071[g]	2.597[g] 2.307[g]	.7119 - 1.627 .6324 - 1.445

8. Bulk Modulus of Elasticity of Ice E (10^9 N/m^2)	1.7 - 9.0[h]	4.1[h]	3.097[b]	.3441 - 1.822
9. Rigidity or Shear Modulus of Ice G (10^9 N/m^2)	3.36-3.8[j]	3.5[j]	1.032[b]	.2701 - .3007
10. Poisson's Ratio σ	.30 - .36[i]	.33[i]	.5[b]	1.389 - 1.667
11. Plate Thickness h (m)	.5 - 6.0[c]	2.5[c]	.0063[d]	.0011 - .0126
12. Velocity Ratio c_2/c_1	1.414-2.639[g]	2.34[g]	1.467[g] 1.293[g]	.5447 - 1.037 .490 - .9144
13. Temperature T, °C	-1.6 - -1.8[h]	-1.7[h]	20[d]	*

a. Meyers et al., 1969.
b. based upon Tk Solver Plus calculations described in Appendix A
c. Ackley et al., 1976.
d. Experimentally determined value.
e. Diachok, 1974.
f. Vidmar, 1987.
g. calculated value based upon previous values in the table
h. Weeks, 1976.
i. Shwartz and Weeks, 1977.
j. Hobbs, 1974.

1. MODEL OF SMOOTH ARCTIC ICE

Acrylic of .63 cm thickness (1/4 inch) was employed to model the Arctic ice pack. Three separate pieces were used: a 20 cm by 40 cm rectangle, a 40 cm square, and a 60.5 cm by 81 cm rectangle. The use of three acrylic pieces along with two different tank environments permitted an increase in the range of geometrical configurations possible and, therefore, data collection over a broader range of angles, which generated more insightful results.

Once a model was found which accurately reproduced the physical parameters of the Arctic, it was necessary to scale the model length and laboratory wavelengths to simulate Arctic frequencies of interest. As indicated, the choice of acrylic ensured close correspondence of the acoustically significant properties. The subsequent concern was assuring that the ratio of plate thickness (h) to acoustic wavelength (lambda) be the same for the acr··· as for the Arctic region being modeled. The accuracy or this scaling technique has been successfully demonstrated (as previously cited) and requires only that this ratio be maintained for the model to be an accurate environmental representation.

Therefore, if a typical Arctic level ice thickness is taken to be 2.5 m, then .0063 m acrylic (1/4 in)

corresponds to a scale of 396.8 : 1. Thus, for the six frequencies chosen, $f_{ice} = f_{acrylic}/396.8$ and:

$f_{acrylic}$ =	20.51 kHz	represents	f_{ice} =	51.68 Hz
$f_{acrylic}$ =	61.52 kHz	represents	f_{ice} =	155.05 Hz
$f_{acrylic}$ =	80.08 kHz	represents	f_{ice} =	201.81 Hz
$f_{acrylic}$ =	123.05 kHz	represents	f_{ice} =	310.11 Hz
$f_{acrylic}$ =	205.08 kHz	represents	f_{ice} =	516.83 Hz
$f_{acrylic}$ =	287.00 kHz	represents	f_{ice} =	723.29 Hz

These frequencies were chosen with attention to the harmonics of the two prevalent operational frequencies, 50 and 60 Hz. They are also distributed over a fairly large range in order to permit investigation of the existence of frequency dependence for reflection and scattering phenomena. The first, third, fourth, sixth, tenth, and fourteenth harmonics of a 50 Hz signal are fairly closely represented. The fifth and twelfth harmonics of a 60 Hz signal also occur. The 123.05 kHz frequency is of particular interest, as it is a close representation of an important harmonic of both signals. The 287 kHz frequency also closely represents a dual harmonic.

Although the acrylic density was greater than that of the water, surface tension forces were sufficent to sustain its flotation. This was fortuitous as it enabled the experiments to proceed without the addition of any

extraneous substances that would have been solely for support and had no similarity to Arctic structures.

2. MODEL OF ARCTIC PRESSURE RIDGE OR KEEL

The pressure ridges present in the Arctic were modeled in the laboratory for scattering data collection. Two separate acrylic keel models were constructed (widths 20 cm and 40 cm) again to expand the range of geometrical configurations (Figure 7). The contribution of the sail to scattering effects is considered negligible (Browne, 1987), thus a sail was not added to the keel model.

Maintaining the same thickness-to-wavelength ratios that were employed for the plane acrylic surface, this model represents a keel of depth 9.12 m and 33.5 m width as indicated by the values in parentheses in Figure 7. This is a standard value for an Arctic pressure ridge and agrees with values reported by Hibler et al. (1974) and previously cited.

The two pressure-ridge keels were constructed by the gluing of a triangular acrylic keel section to the plate acrylic sheet. This was performed using Comstik Plexite Cement 1 adhesive manufactured by the Rohm and Haas Company. As the scattering effects of the acrylic keel are the interactions of interest, any alteration of the acoustic properties of the acrylic by this minute glue layer were ignored.

Environmental Structure and Laboratory Model Counterpart

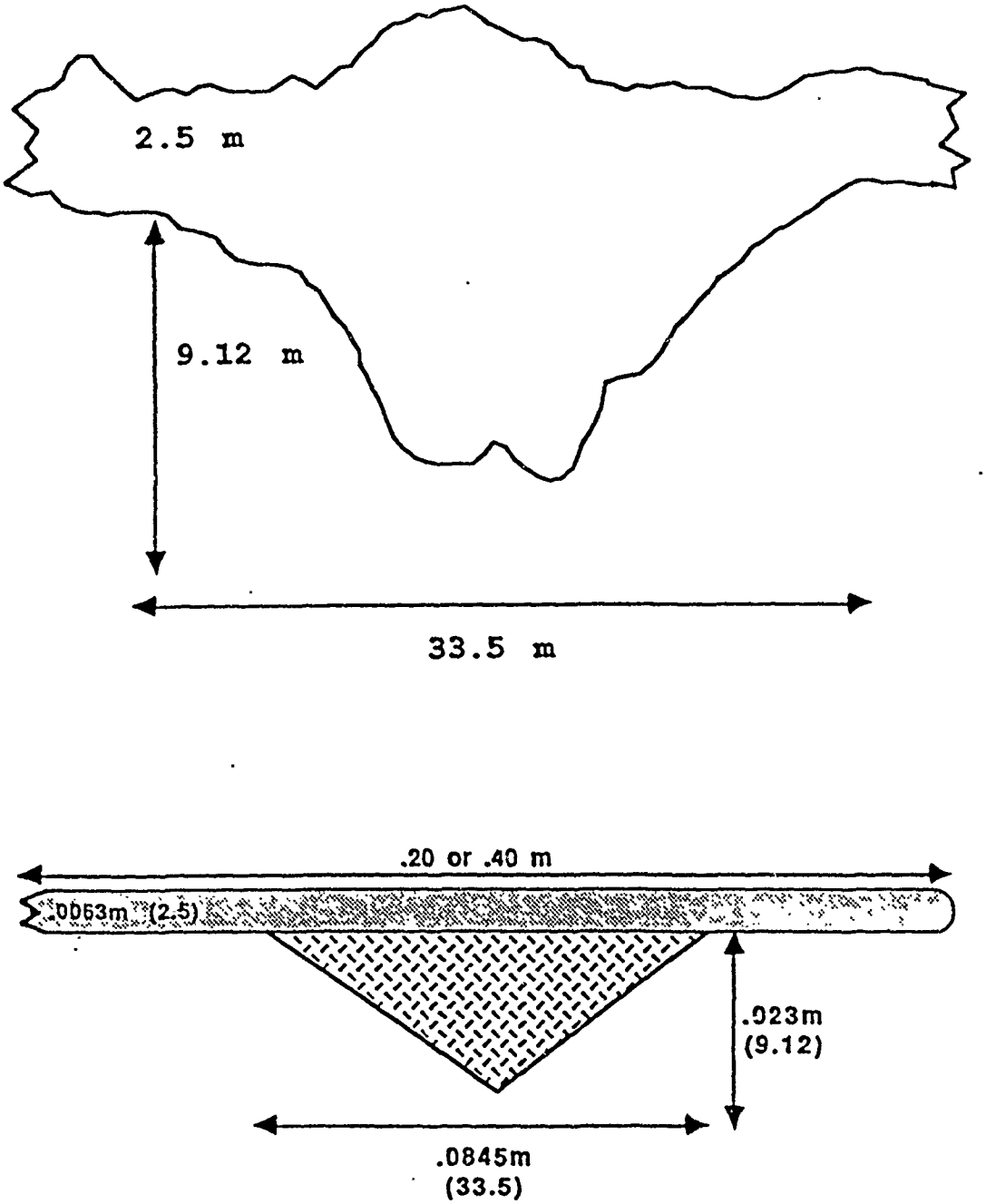

Figure 7. A schematic diagram of the laboratory model and a depiction of the structure it represents with appropriate dimensional values.

C. EXPERIMENTAL TECHNIQUE

1. INITIAL ASSUMPTIONS

It was necessary to make several assumptions at the outset of the experiment to simplify the model. Attenuation effects in the fluid were determined to be negligible, due to the similarity of path lengths between the direct and reflected pulses. Any loss occurring would affect the transmission of both waves virtually equally so that these effects can be factored out.

Additionally, homogeneity of the acrylic properties was assumed. This, of itself, is a valid conclusion, but it contradicts the known anisotropy of Arctic sea ice which the model represents. Likewise, the salinity and temperature structure of the sea water layer immediately adjacent to the pack ice demonstrates vertical variation due to salt precipitation and mixing effects (see Figure 3). The homogeneity of the laboratory model again does not correspond to the environmental values. These limitations in the model were noted but deemed negligible when studying solely the interactions that occur at the interface of the two media.

The final assumption was that the experiment occurred in the acoustic far field. This condition reduced the model to plane waves, thereby simplifying computation. This assumption requires that the separation between

hydrophones be sufficient to allow for curvature effects in the propagating wavefront to be negligible. This is usually assured by satisfying:

$$kr >> 1$$

where k is the wave number ($2\pi f/c$) and c is the speed of sound in the medium, f is the frequency of the waves and r is the separation of the source and the point of concern in meters. In order for the product kr to be considered much greater than one, the condition is placed that kr should be greater than 11. Taking a value of kr equal to 11, c = 1500, and solving for r using the lowest frequency (f = 20.51 kHz), (which will cause the maximum value for r within which the experiment would still be operating in the near field), generates r = .128 m. Thus, in order for the experiment to be considered in the far field r (the separation between source and receiver) must be greater than 12.8 cm. With a minimum hydrophone separation in excess of 20 cm, this value was exceeded throughout the experiment. The far field assumption is therefore valid.

2. PRELIMINARY COMPUTATIONS

Initial calculation of sound speed in the water and acrylic both theoretically and experimentally was essential for the remainder of the computations. Wilson's simplified equation:

$$c = 1449.2 + 4.6T - .055T^2 + .00029T^3 + (1.34 - .01T)(S-35) + .016z$$

where c = sound speed (m/s) T = temperature (°C)

S = salinity (ppt) z = depth (m)

presented the theoretical value for sound speed of water (Clay and Medwin, 1977). When combined with laboratory measurements and literature parameters, a value for sound speed in water of 1500 m/s was determined to be reasonable.

Theoretical computation of the acrylic sound speed was difficult due to the lack of available acoustically oriented data. Thus, fundamental equations were employed with an iterative solving process to acheive a sound speed value of 2201.09 m/s which compared favorably with laboratory determinations. The mathematical process utilized is detailed in the Appendix.

Pulsed omnidirectional signals of two cycle duration were transmitted and the reflection was identified and isolated employing a precalculated time reference "window". Measurement of precise hydrophone placement relative to the boundaries of the tank and knowledge of the value of the sound speed allowed this parameter to be computed. A simple series of trigonometric and velocity equations were used. The Appendix also discusses more fully the manner in which this time window was determined.

Figure 8 is a sample return with annotated pulses. It is indicative of the type and format of data collected. It also demonstrates the specific parameters which were chosen for data collection during the experiment.

D. DATA COLLECTION METHODS

1. REFLECTION DATA COLLECTION

Once the variable channel mode had been selected and all extraneous or residual pressure phenomena in the tank had subsided, the trigger was activated, emitting the two cycle pulse as described above. This was viewed on the upper trace of Figure 8 (denoted channel B) while all reflections were displayed on the lower trace as shown in Figure 8 (channel A).

The direct path and reflected pulse were isolated employing the time window parameters determined as per the Appendix. The direct path was obviously the first to arrive; the desired surface reflected path was isolated from the remaining "noise" reflections. The Rapid Systems software gives time and voltage output for both channels at distinct time positions along the waveform. These locations are chosen by means of a cursor along the ordinate axis.

Measurement was taken of the peak voltage for the direct path pulse and the reflected pulse. The direct path

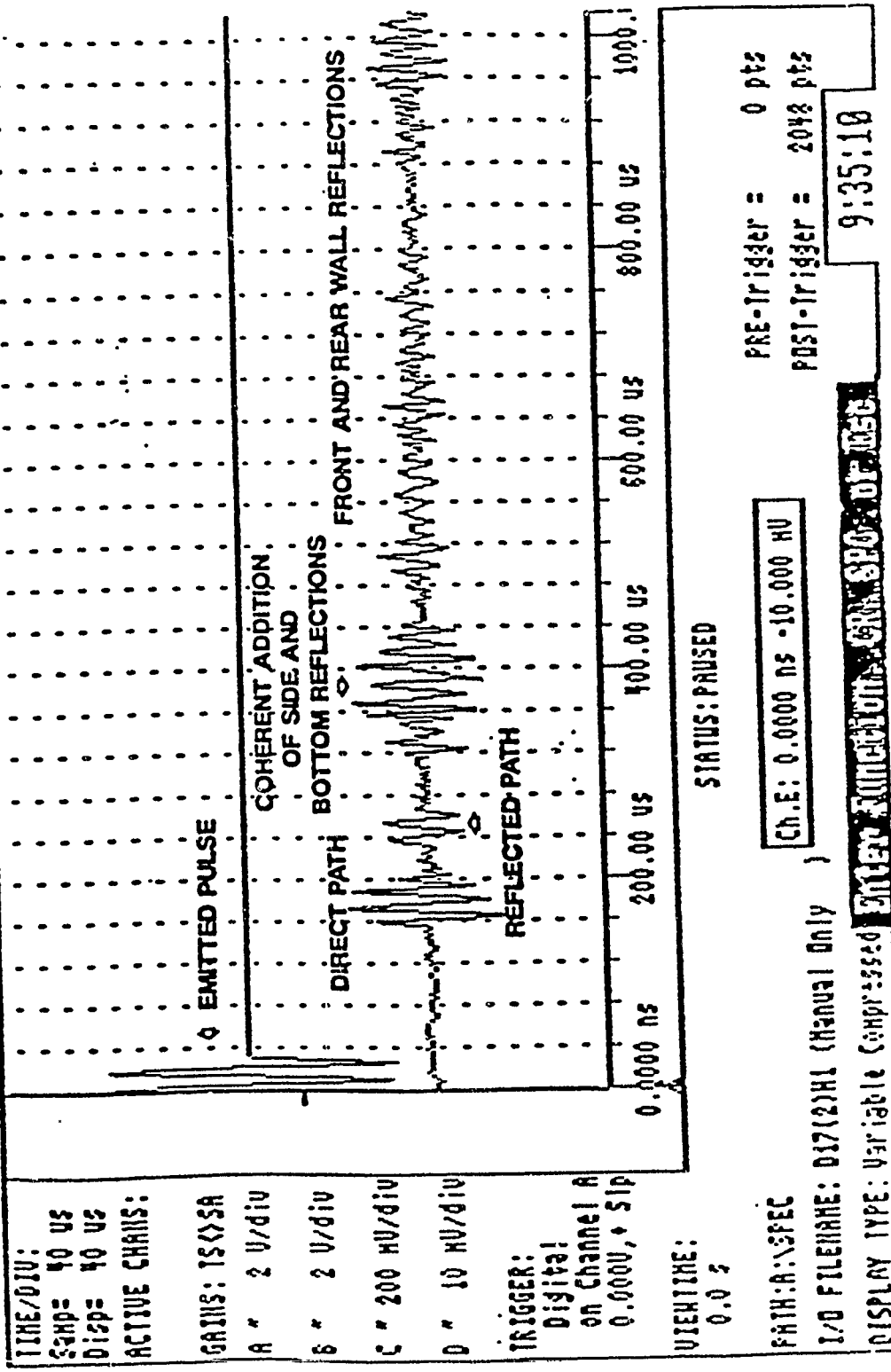

Figure 8. Typical format for data collection with annotations indicating the echoes of import

value served as the denominator for the reflection ratio and the numerator was the peak voltage amplitude of the reflected pulse. Thus, the ratio generated is a pressure reflection coefficient. This method inherently has some limitations due to the stepping mechanism of the voltage reading system. The software proceeds along the waveform in increments of 2 microseconds. It is therefore possible that the actual peak values of either of the signals might have occurred in between the samplings and been overlooked. This possibility was accounted for by the performance of a minimum of six "runs" at each geometry (i.e. each angle of incidence) for each frequency and the computation of an average value for both direct path voltage and reflected voltage. This average value serves as one "trial" and corresponds to a specific voltage and specific angle of incidence. The voltage ratio (representing the pressure ratio) was then plotted as the pressure reflection coefficeient.

2. SCATTERING DATA COLLECTION

The initial goal was collection of both forward and backscatter data from the acrylic keel models. One hydrophone was placed adjacent to and in contact with the source and a second was placed on the opposite side of the acrylic, equidistant from the keel and at the same depth as the source. Due to the ringing that occurs from the

magnitude of the power of the emitted burst, the hydrophone was rendered inutile for reception of backscattering data. Some separation of the source and receiver hydrophone is required and this precluded obtaining backscatter data due to a desire to maintain appropriate angular alignment.

Forwardscatter data was collected in a manner similar to that followed for the reflection experiment. A diagram of the model configuration is found in Figure 9. A minimum of twenty runs was performed for each trial. The value at each trial represents the pressure scattering coefficient, a ratio of forwardscatter pressure to direct path pressure at a given angle of incidence. It is, however, more common to work with grazing angle when dealing with scattering data. The grazing angle is the angle of impingement measured from the horizontal, or the complement of the angle of incidence. Thus, data are presented in this format.

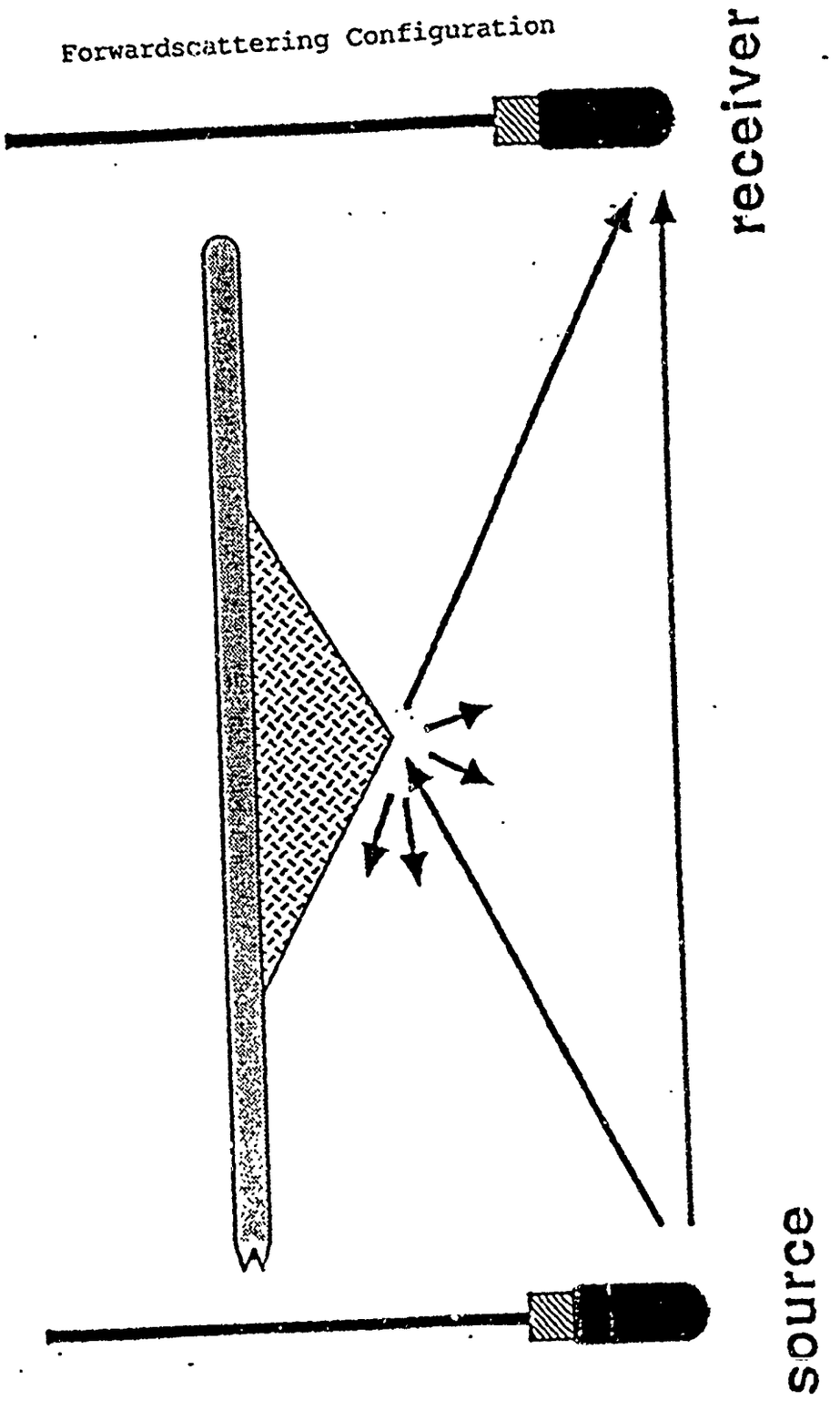

Figure 9. Hydrophone and acrylic model configuration for gathering forwardscattering data

IV. ACOUSTIC REFLECTION

A. THEORETICAL FOUNDATIONS

Initial understanding of wave propagation may be gained through a study of Huygens' principle. This states that each discrete unit area on an advancing wave is considered a re-radiating point source of spherical waves. The outer surface that includes these new "wavefronts" constitutes the front of the new wave (Figure 10).

Huygen's theory may be expanded to explain the reflection of a wave at a plane interface. The wave construction proceeds with the supposition that there exists an "image" source at a distance beneath the surface which is equivalent to the distance between the surface and the real source. The real wave front is assumed to travel into the image region as in Figure 10(a). Concurrent with the propagation of the real wave, the image wave originates at the image point (Figure 10(b)) and travels towards real space, entering it to become the reflected wave. The reflected wave will have an intensity of $R_I I$ where I is the intensity of the incident wave and R_I is the intensity reflection coefficient, which represents that fraction of the intensity of the incident wave that is reflected. The reflected wave continues to propagate in the real region in the same manner as the original wave (Figure 10(c) (Clay and Medwin, 1977).

Huygen's Principle As Applied To Reflection Phenomena

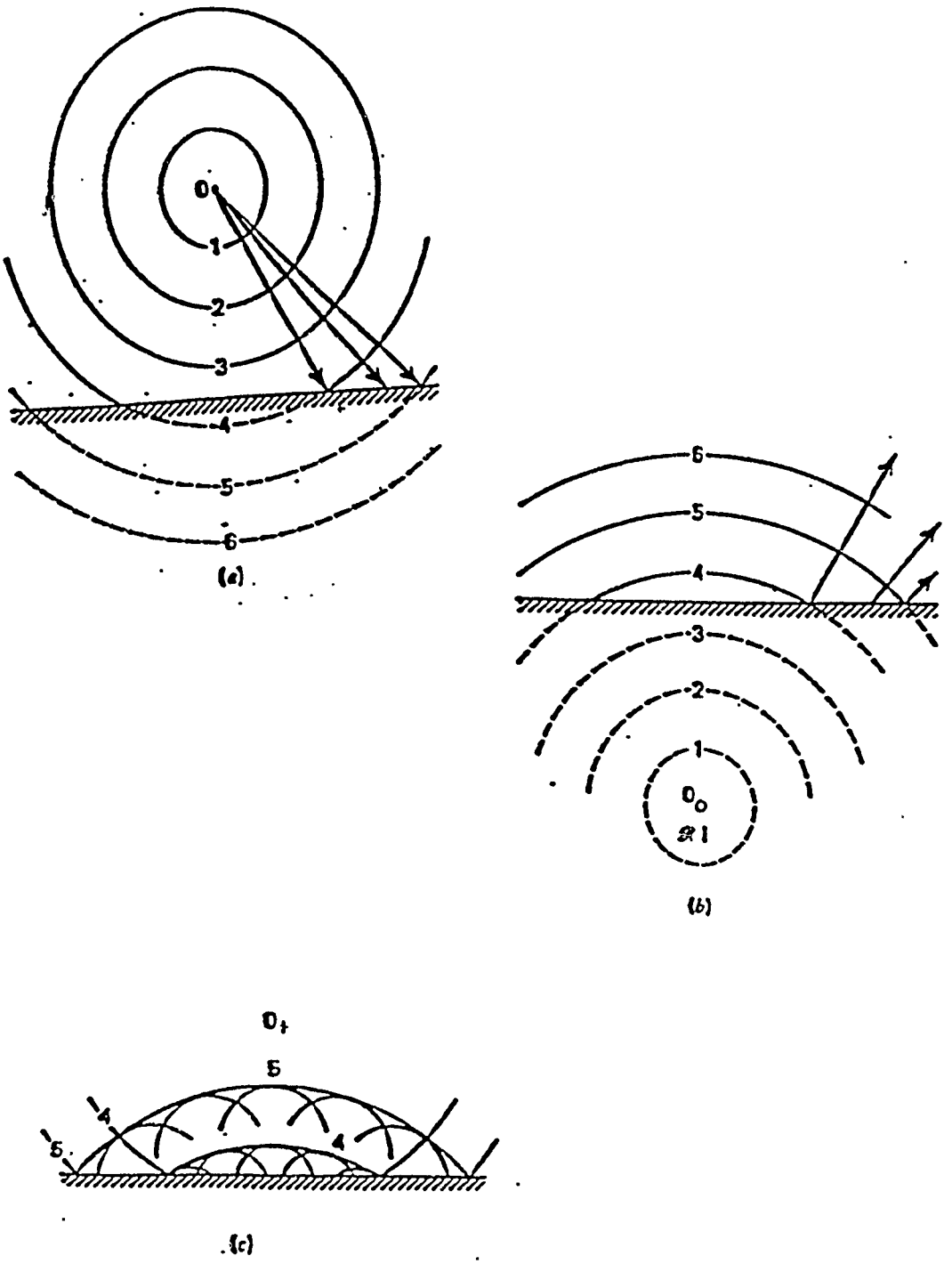

Figure 10. (a) Propagation of the real wave front into the "image" region. (b) concurrent propagation of the image wave towards and then into the real region. (c) the final observed effect. (Clay and Medwin, 1977)

In the study of acoustics, it is common to deal with large distances from the source. In this region, termed the far field, the curvature of the wave is relatively small, in fact negligible. Thus, the wave may be considered a plane phenomenon. The mathematical basis for and limitations to this assumption are described in the Procedure chapter.

The use of ray theory further simplifies acoustic energy analysis. A line constructed perpendicular to the wave fronts is traced as a ray rather than tracking the paths of individual waves (Figure 10(a)). It is with these theoretical assumptions that the discussion shall proceed.

B. WAVE PROPAGATION AT AN IMPEDANCE INTERFACE

When acoustic waves strike a discontinuity of acoustic impedance (Z), whether it be caused by a change in medium density (ρ) or sound velocity (c) or both, the propagation is altered. At the interface of a plane smooth boundary, part of the energy is transmitted and a portion of it is reflected. The angle at which the energy is reflected is identical to the angle of incidence. The transmitted wave, however, follows Snell's Law:

$$\{\sin(\theta_1)/c_1\} = \{\sin(\theta_2)/c_2\} \qquad (1)$$

where c_1 and c_2 are the sound speeds in the respective media, θ_1 is the angle of incidence in medium 1 measured from the normal, and θ_2 is the transmitted angle in medium 2, also measured from the normal.

Figure 11 represents the interaction at an acoustic impedance interface. Notice that θ_1, the incident angle is equal to θ_r the reflected angle. Also note that in employing Snell's Law, one can determine that the sound speed of medium 2 must be lower than that of medium 1. This fact is derived from the refraction of the transmitted ray toward the perpendicular and the decrease in θ_2 from θ_1.

Acoustic waves travel as a pressure disturbance as previously indicated. The value of the reflection coefficient will therefore be the ratio of the reflected pressure amplitude to the incident pressure. In order to calculate this ratio two boundary conditions are required. They are:

1. Continuity of Pressure: The interface does not have an excess pressure on one side or the other. This requires that the algebraic sum of the incident and reflected pressures be equal to the transmitted pressure at the interface.

2. Continuity of the normal component of the fluid particle velocity: The two media maintain contact at the

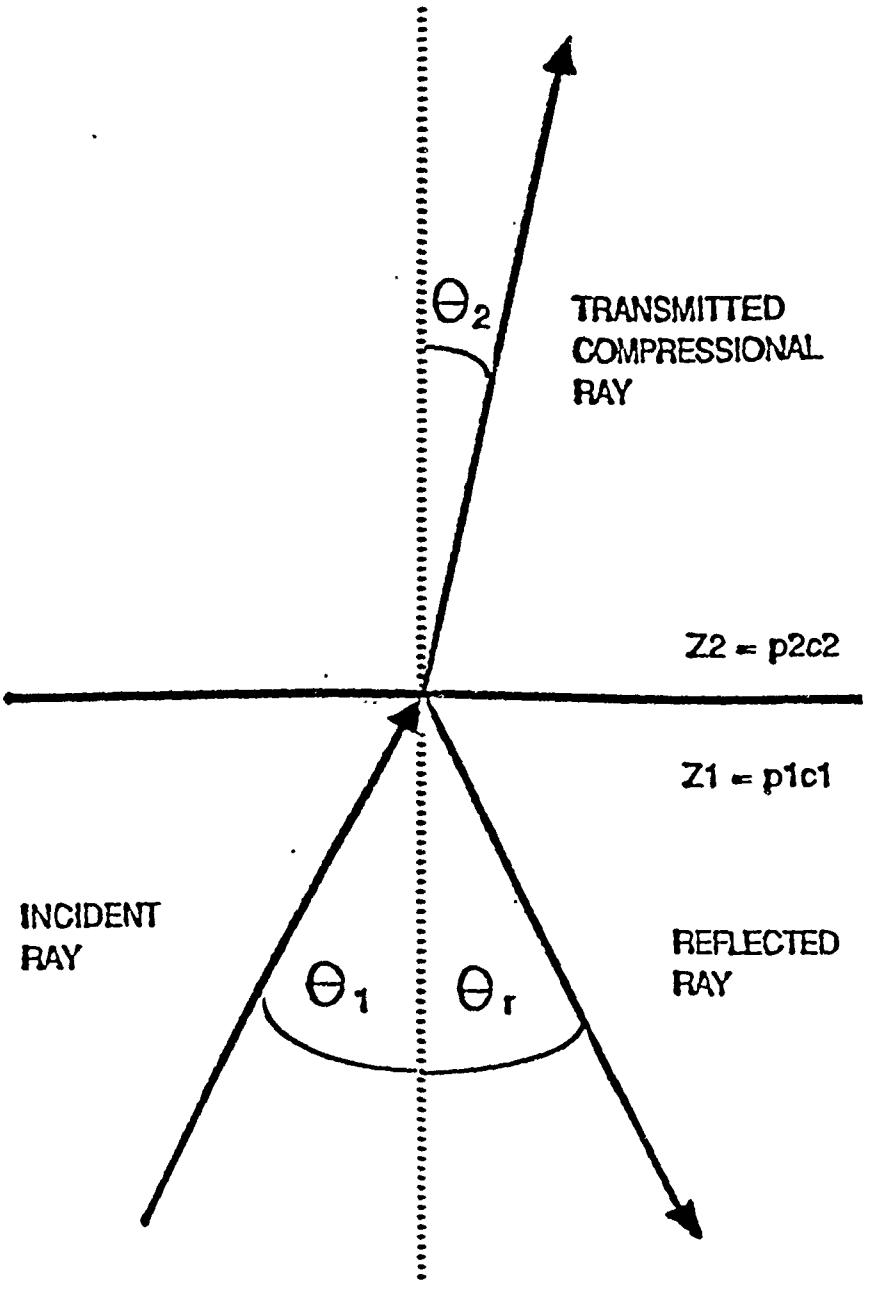

Figure 11. Acoustic interaction at the interface between two media of differing acoustic impedances. A portion of the energy is transmitted into the new medium, the remainder is reflected back into the medium of origin

interface as the signal reflects and passes through the interface.

Once these conditions are satisfied, the ratio of reflected to incident pressure (R_p) may be determined. This is:

$$R_p = \frac{p_2\ c_2 - p_1\ c_1}{p_2\ c_2 + p_1\ c_1} = \frac{\mathbf{p}_r}{\mathbf{p}_i} \qquad (2)$$

where $p1$ and $p2$ are the densities of the respective media, $\mathbf{p}_r$ is the amplitude of the reflected pressure and $\mathbf{p}_i$ is the incident pressure amplitude. Taking into account oblique angles of incidence leads to:

$$R_p = \frac{p_2\ c_2 \cos(\theta_1) - p_1\ c_1 \cos(\theta_2)}{p_2\ c_2 \cos(\theta_1) + p_1\ c_1 \cos(\theta_2)} = \frac{\mathbf{p}_r}{\mathbf{p}_i} \qquad (3)$$

A plot of equation (3) with typical acrylic values is shown in Figure 12. These values are c_1 = 1500 m/s, c_2 = 2201.09 m/s, p_1 = 998.503 kg/m^3, and p_2 = 1189.8 kg/m^3.

As long as $c_2 < c_1$, the value of $(c_2/c_1)\sin(\theta_1)$ will be less than one for all values of θ. However, if $c_2 > c_1$, as is true in the Arctic and the acrylic model, the phenomenon of "total reflection" occurs. A critical angle (θ_{crit}) is reached when:

$$\sin(\theta_{crit}) = (c_1/c_2) \qquad (4)$$

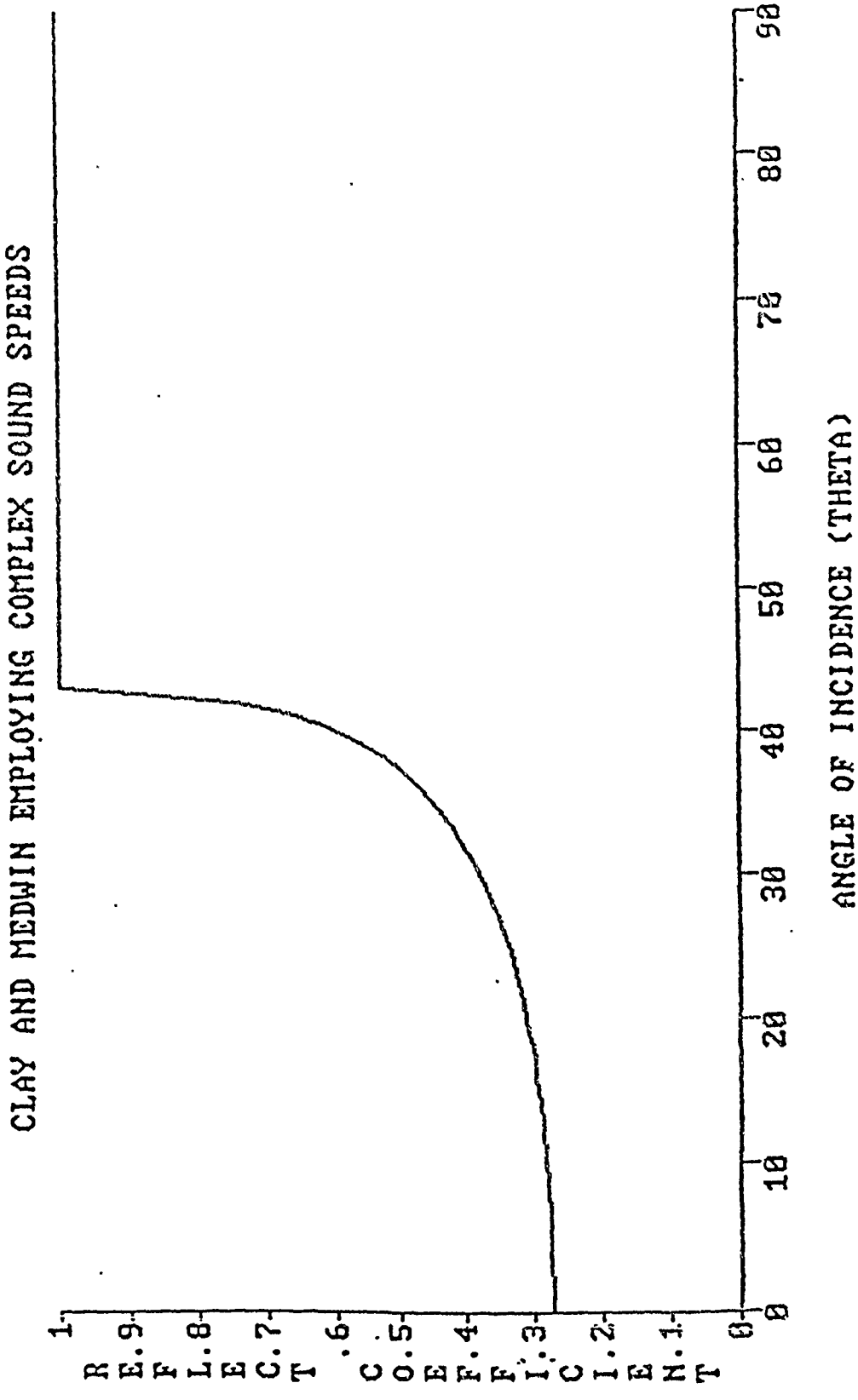

Figure 12. The theoretical pressure reflection coefficient at the acrylic-water interface employing equation (3)

At angles greater than the critical angle, the signal reflects with a pressure reflection coefficient of one and an associated phase change. To indicate this and to resolve ambiguity caused by the value of $(c_2/c_1)\sin(\theta_1)$ exceeding one, complex notation is employed and results in:

$$R_p = \frac{p_2\ c_2\ \cos(\theta_1) + i\ p_1\ c_1\ b_2}{p_2\ c_2\ \cos(\theta_1) - i\ p_1\ c_1\ b_2} \qquad (5)$$

where $b_2 = \pm i\ \cos(\theta_2) = \sqrt{(c_2/c_1)^2\ \sin^2(\theta_1) - 1}$

(Clay and Medwin, 1977). This equation is depicted in Figure 13 employing typical model values as in Figure 12.

C. REFLECTION AT A FLUID-SOLID BOUNDARY

In the Arctic a more complex case is of concern. This region experiences a plane wave incident upon what is normally modeled as a plane boundary between a liquid halfspace and a solid one. Obviously this liquid-solid model is not as simple as the reflection at an interface between two fluids differing solely in density or sound speed, yet still not as complex as the Arctic in which the ice is actually a rough-surfaced lossy multi-layered viscoelastic medium upperbounded by a gas. Unlike the liquid or gas, the solid phase can support shear or transverse waves; this adds another dimension to the

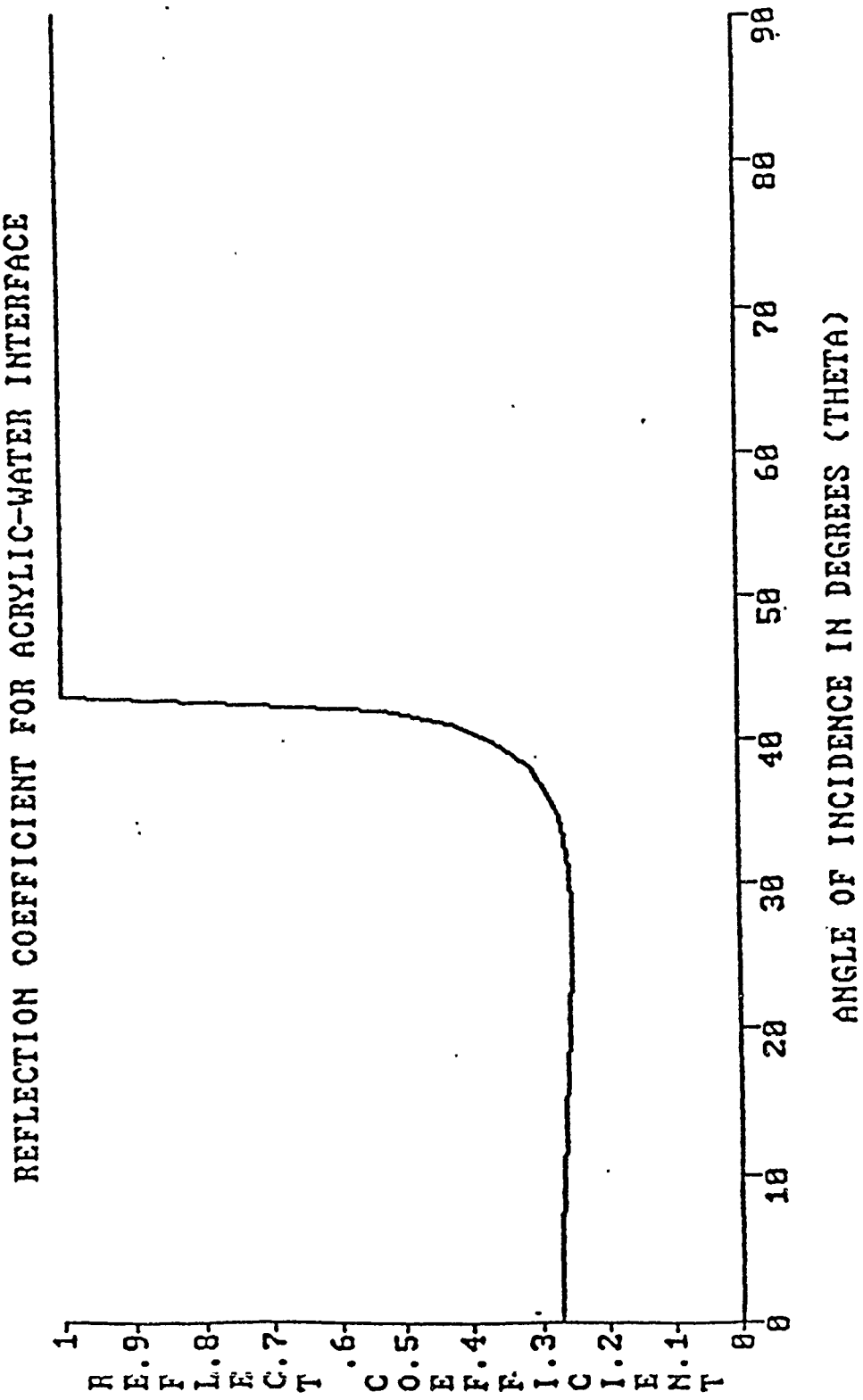

Figure 13. A depiction of the theoretical pressure reflection coefficient derived from equation (5) when using laboratory values

increasingly diverse reflection picture. When a compressional wave in a fluid is incident on an elastic solid, part of the energy is reflected back into the liquid medium, part is transmitted as a compressional wave in the solid, and part is transmitted as a shear wave in the solid.

At the liquid/solid boundary, the vertical displacements in the two media are equal, the vertical stress is continuous, and the tangential stress in the solid vanishes at the interface because the non-viscous liquid (which water is assumed to be) does not support shear waves. Snell's Law remains applicable and may be expanded to:

$$\{\sin(\theta_1)/c_1\} = \{\sin(\theta_{2p})/c_{p2}\} = \{\sin(\theta_{2s})/c_{s2}\} \qquad (6)$$

where c_{p2} is the compressional sound speed in medium 2, c_{s2} is the shear sound speed in medium 2, θ_{2s} is angle of shear wave propagation in medium 2 measured from the normal and θ_{2p} is angle of compressional wave propagation in medium 2 measured from the normal. This, according to Clay and Medwin (1977), (given the same boundary conditions as the liquid-liquid interface), alters the equation for the pressure reflection coefficient to equation (7):

$$R_p = \frac{4\tau_2\delta_2\alpha^2 + (\delta_2^2 - \alpha^2)^2 - (p_1/p_2)(\tau_2/\tau_1)(w^4/c_{s2}^4)}{4\tau_2\delta_2\alpha^2 + (\delta_2^2 - \alpha^2)^2 + (p_1/p_2)(\tau_2/\tau_1)(w^4/c_{s2}^4)}$$

where simplifying by algebraic manipulation leads to:

$$w = 2\pi f \quad (f \text{ is frequency in Hertz})$$

$$\alpha = (w/c_1)\sin(\theta_1) \qquad \tau_1 = (w/c_1)\cos(\theta_1)$$

$$\tau_2 = (w/c_{p2})[1 - \{(c_{p2}/c_1)\sin(\theta_1)\}^2]^{1/2}$$

$$\delta_2 = (w/c_{s2})[1 - \{(c_{s2}/c_1)\sin(\theta_1)\}^2]^{1/2}$$

This form of the reflection coefficient takes into account the additional losses observed due to the propagation of shear waves, which the liquid is unable to support. Figure 14 demonstrates the ray geometry in this environment, the difference from Figure 11 being the transmission of a shear wave in addition to a compressional wave.

Above the critical angle it is necessary to utilize complex notation. This results in a plot for the pressure reflection coefficient in terms of incident angle (with the acrylic model values) as shown in Figure 15. Note that the value of the coefficient is unity both at the critical angle and at normal incidence. Values of the reflection coefficient for incident angles less than the critical angle (θ_{crit}) are affected by alterations of the compressional wave speed (c_p), whereas those greater than θ_{crit} are affected by variations of shear celerity (c_s).

Acoustic Interaction At A Liquid- Solid Interface

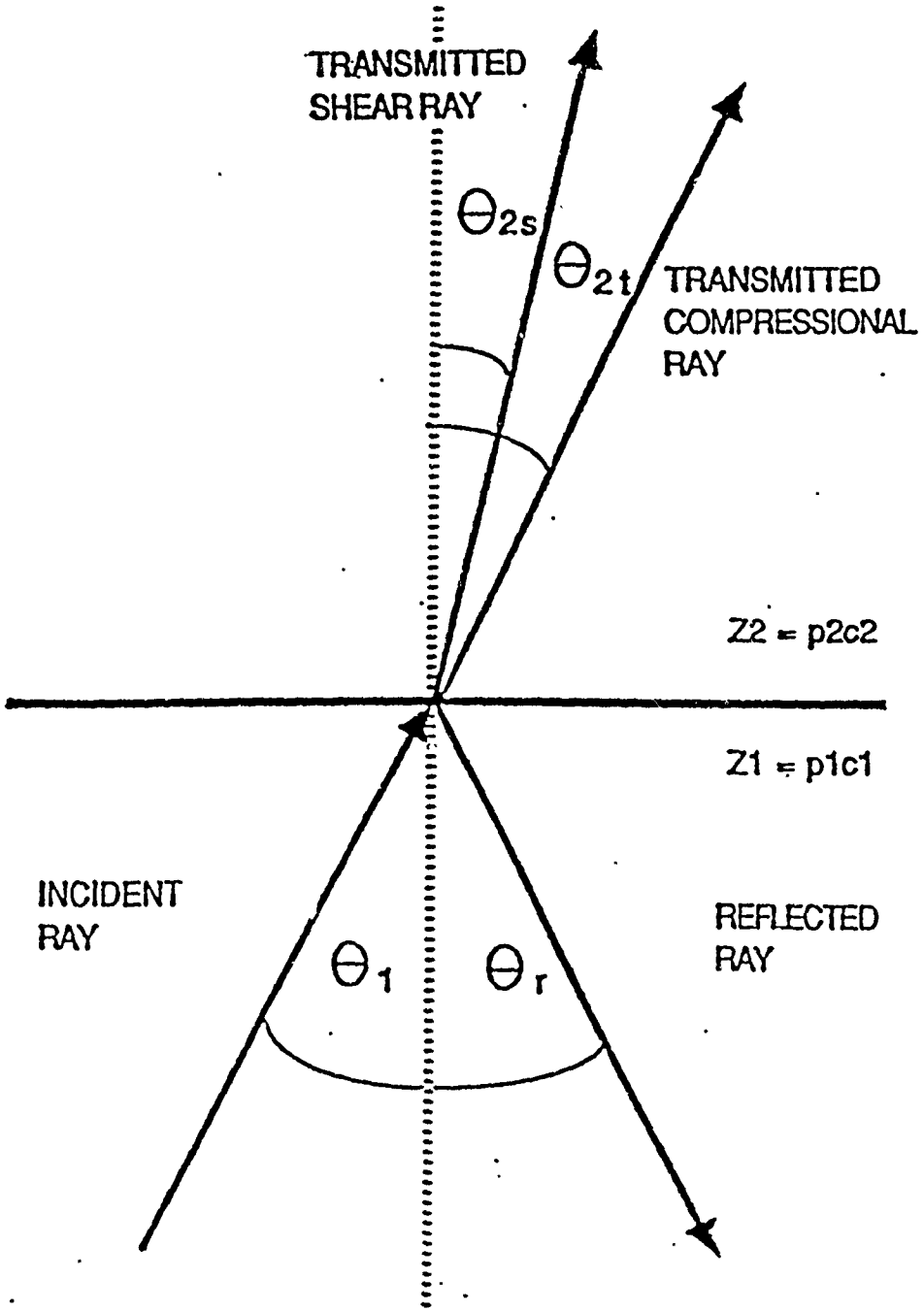

Figure 14. Acoustic interaction at the interface between a liquid and solid. Energy is transmitted as both compressional and shear waves as well as reflected

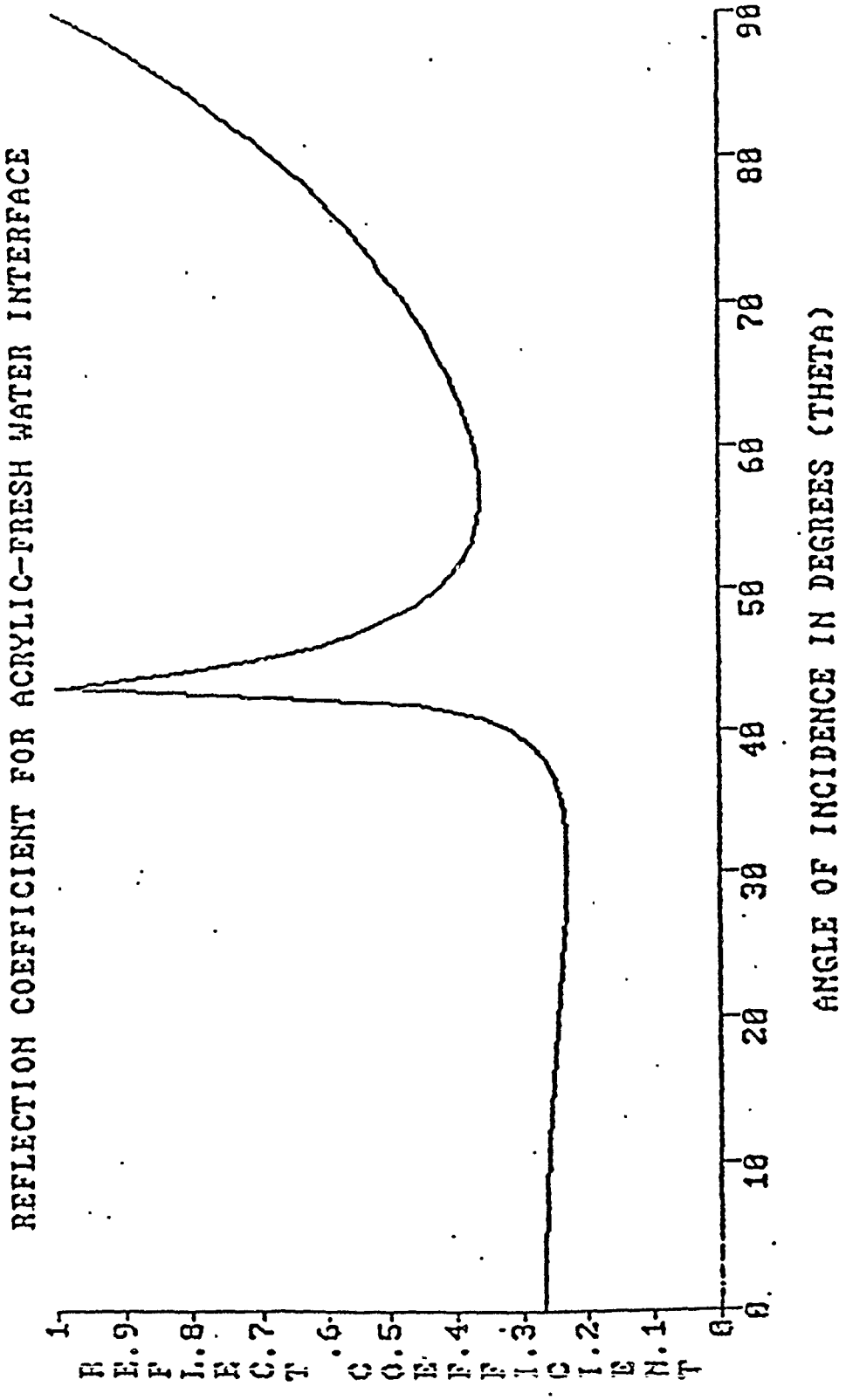

Figure 15. A plot of the theoretical pressure reflection coefficient obtained from equation (7) when complex celerities are used above θ_{crit}

Although frequency may be factored from Clay and Medwin's equation (7), a frequency dependence is noted from the experimental data; this is attributed to acoustic energy attenuation in the media. Velocity and attenuation in solids change with frequency according to Vidmar (1987) and McCammon and McDaniel (1985) although these conclusions were not obtained by Langleben (1970) for sea ice. Attenuation effects are normally modeled mathematically by the utilization of complex sound speeds.

To generate a complex celerity, the real sound speed c is redefined as $c = c' + ic''$ with both c' and c'' real numbers. Subsequently, c' and c'' are defined as follows:

$$c' = c \,/\, [1 + (\alpha/k)^2] \quad \text{and}$$
$$c'' = [c\,(\alpha/k)] \,/\, [1 + (\alpha/k)^2] \qquad (8)$$

where k is the wave number ($2\pi f/c$) and α (alpha) is the compressional attenuation coefficient (Clay and Medwin, 1977). The shear attenuation coefficient will be represented by β. The attenuation coefficient itself often varies with frequency; McCammon and McDaniel (1985) report attenuation coefficients in ice of:

$$\alpha = .06f(-6/T)^{2/3} \text{ dB/m kHz} \quad \text{and}$$
$$\beta = .36f(-6/T)^{2/3} \text{ dB/m kHz}$$

where α is the coefficient for compressional waves, β is the coefficient for shear waves, f is frequency in kHz, and T is temperature in °C.

Employing equation (7) with complex sound celerity to account for observed attenuation, variation in the value of the reflection coefficient occurs relative to that found employing solely real number celerities. The region to the left of the critical angle (θ_{crit}) is affected by the compressional speed attenuation (α) and angles larger than θ_{crit} vary due to alterations in the shear speed attenuation (β). The value of θ_{crit}, however, does not change, and the angle still represents a local maximum of the reflection coefficient, but that value may no longer be unity.

Brekhovskikh (1980) expands the Clay and Medwin approach further by considering a layered medium of finite thickness bounded by two half spaces. This model more closely represents the Arctic environment. His pressure reflection coefficient is defined as:

$$R_p = \frac{M\,(Z_1 - Z_3) + i\,[(M^2 - N^2)\,Z_i + Z_3]}{M\,(Z_1 + Z_3) + i\,[(M^2 - N^2)\,Z_1 - Z_3]}$$

when the following are true:

$$Z_1 = (\rho_1 c_1)/\cos(\theta_1) \qquad Z_2 = (\rho_2 c_{p2})/\cos(\theta_{2p}) \qquad (9)$$

$$Z_{2t} = (\rho_2 c_{s2})/\cos(\theta_{2s}) \qquad Z_3 = (\rho_3 c_3)/\cos(\theta_3)$$

$$M = (Z_2/Z_1)\cos^2(2\theta_{2s})\cot(P) + (Z_{2t}/Z_1)\sin^2(2\theta_{2s})\cot(Q)$$

$$N = \{Z_2 \cos^2(2\theta_{2s})/Z_1 \sin(P)\} + (Z_{2t}/Z_1) \sin^2 2\theta_{2s}/Z_1 \sin(Q)$$

$$P = k_2 h \cos(\theta_{2p}) \qquad Q = K_2 h \cos(\theta_{2s})$$

$$k_2 = 2 \pi f / c_{p2} \qquad K_2 = 2 \pi f / c_{s2}$$

$$h = \text{layer thickness (m)}$$

When adapting equation (9) to the Arctic environment Brekhovskikh obtains a reflection coefficient of unity for all angles. This conclusion is substantiated by McCammon and McDaniel (1985) using the Thompson-Haskell matrix method. Using the values for the acrylic model, a value of one is likewise obtained (Figure 16). However, this does not correspond to real world or laboratory data, a disparity noted by McCammon and McDaniel, as well. The means of solving this incongruity is the inclusion of attenuation into the equation by employing complex sound speeds.

When applied to equation (9) as per McCammon and McDaniel (1985) complex sound speeds and attenuation produce reflection coefficient values less than one. Two samples of the variation this causes are found in Figures 17 and 18.

D. EXPERIMENTAL DATA AND CONCLUSIONS

Figures 19(a) through 19(f), show equation (7) solved for the appropriate frequency and employing the attenuation factors as respectively noted, with

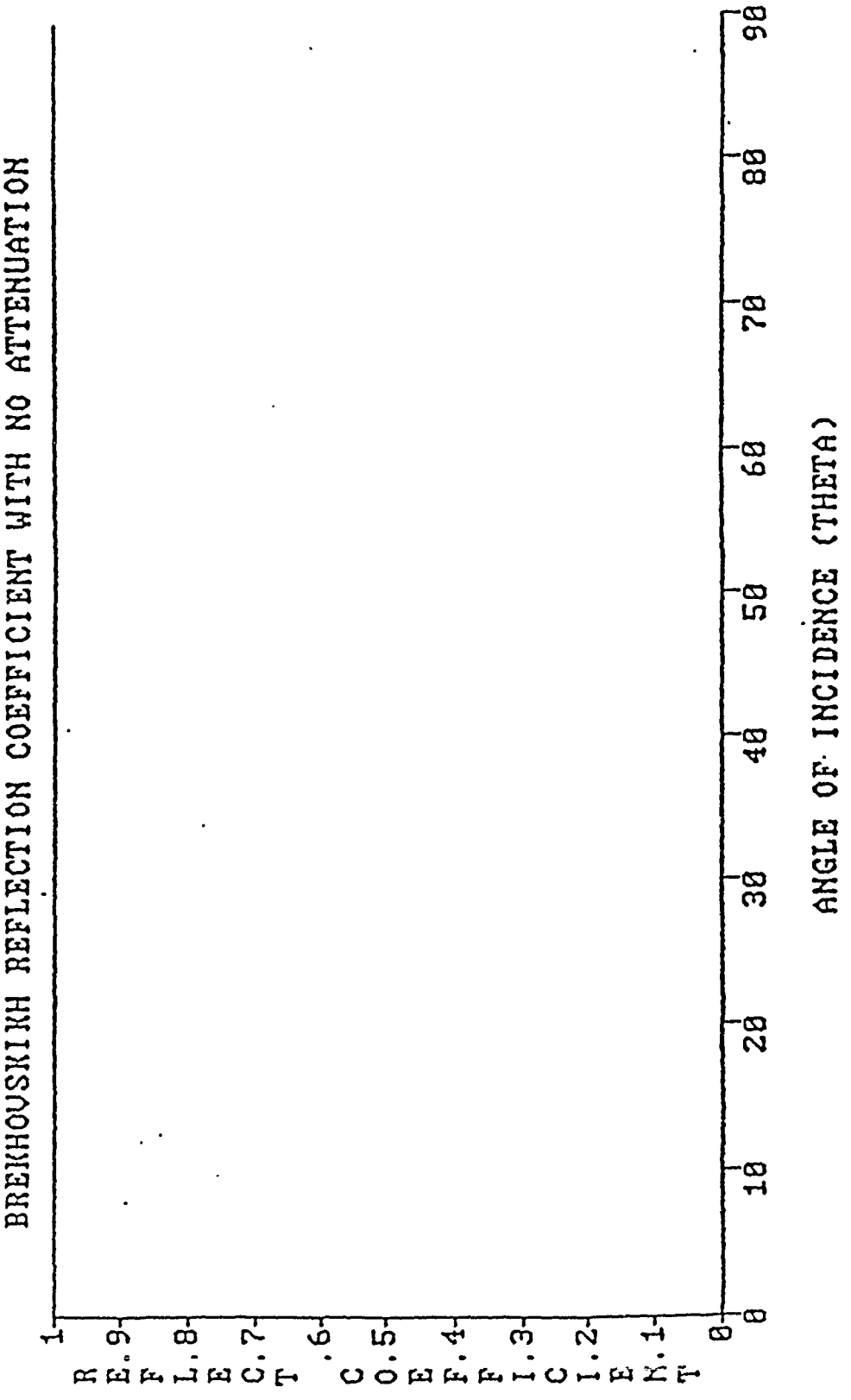

Figure 16. A plot of Brekhovskikh's three-layer equational model for the pressure reflection coefficient employing laboratory values

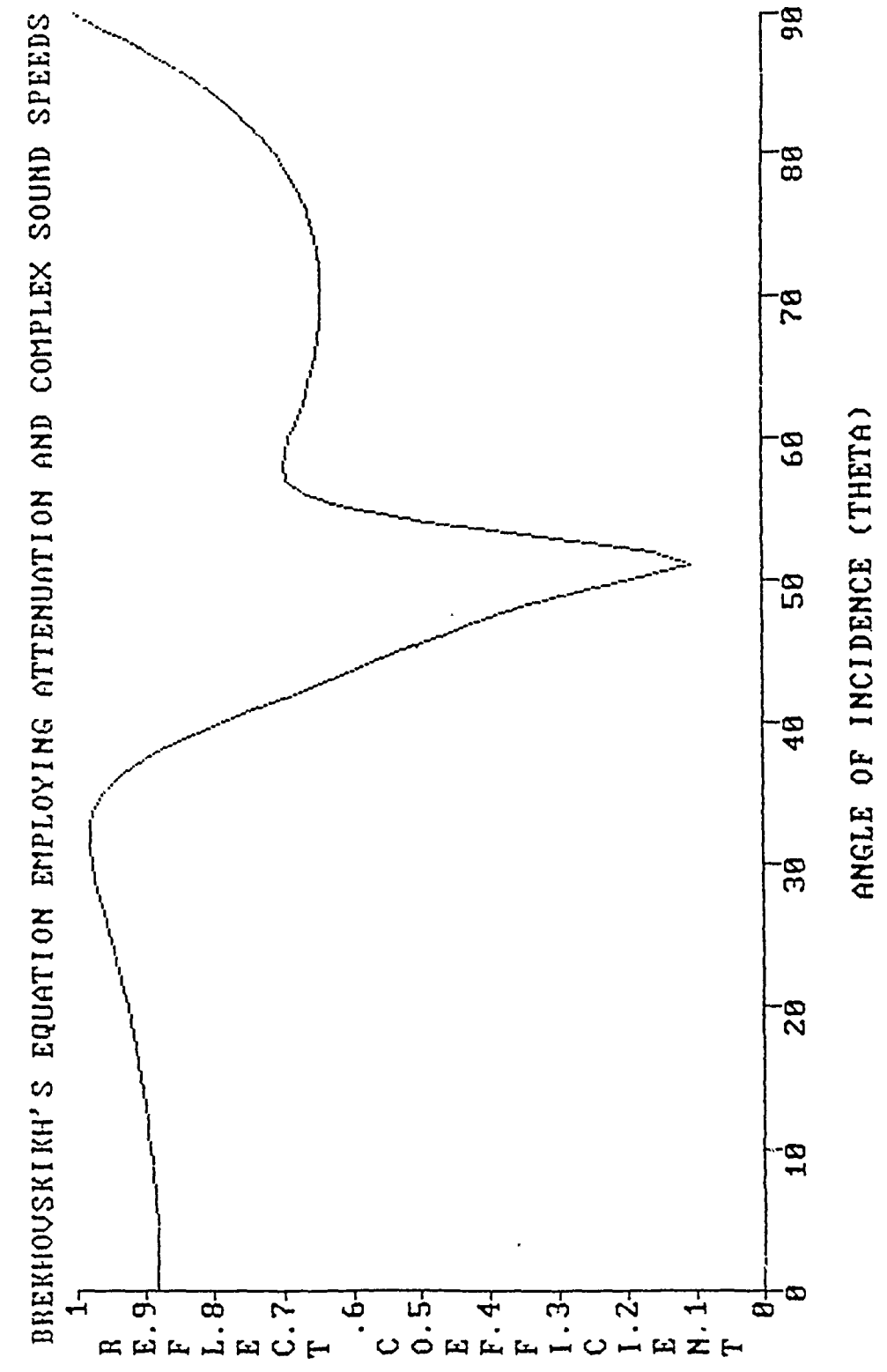

Figure 17. A depiction of Brekhovskikh's equation (9) with $\alpha = -60$, $\beta = -600$ and a frequency of 123.06 kHz

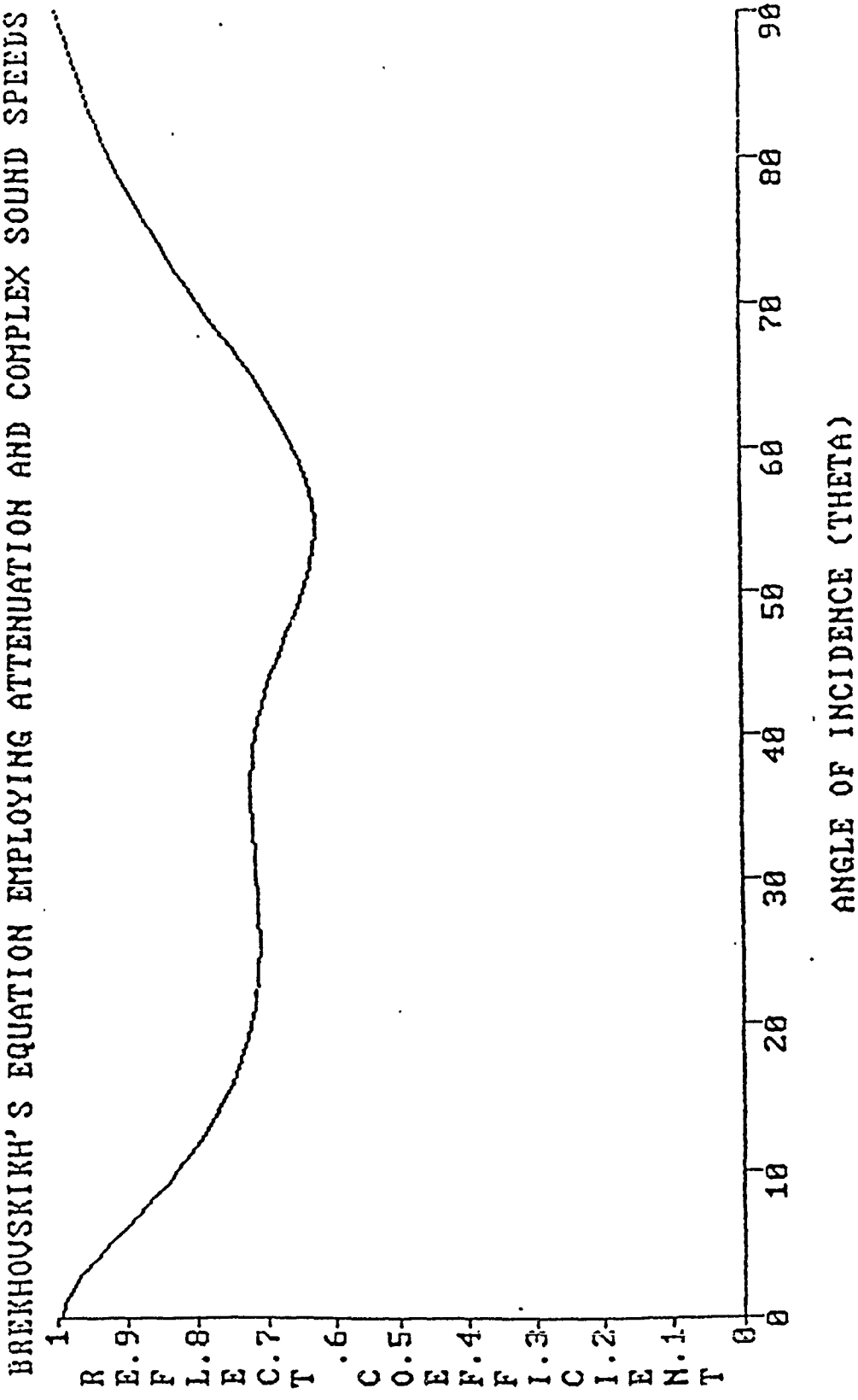

Figure 18. A plot of Brekhovskikh's equation (9) with $\alpha = 125$, $\beta = 400$ and a frequency of 80.08 kHz

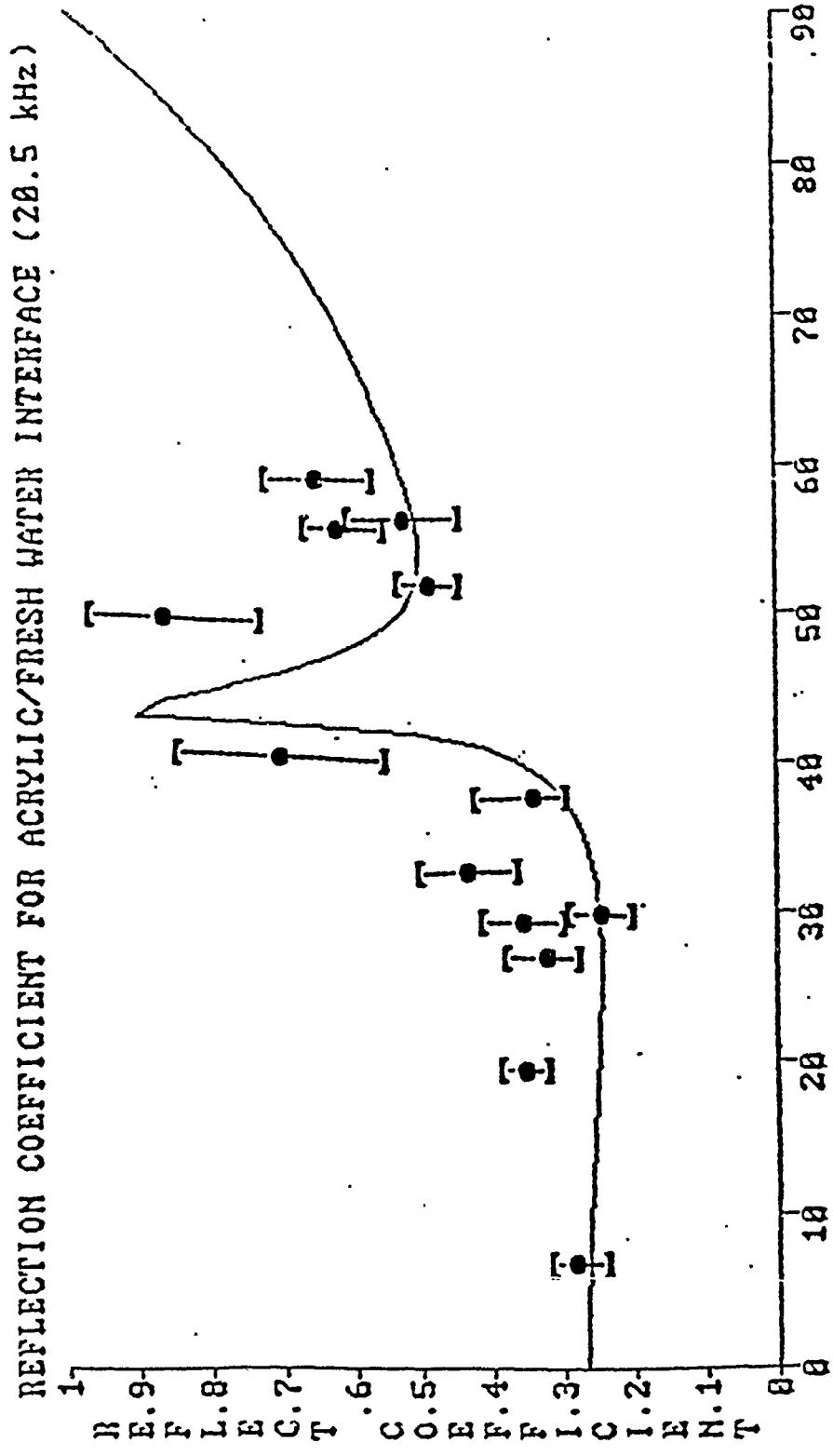

Figure 19(a). The line represents the values of equation (7) plotted with appropriate attenuation factors. The points are experimentally determined mean values with the "error bars" denoting high and low values. This graph is for 20.5 kHz with α = .06 and β = 30.

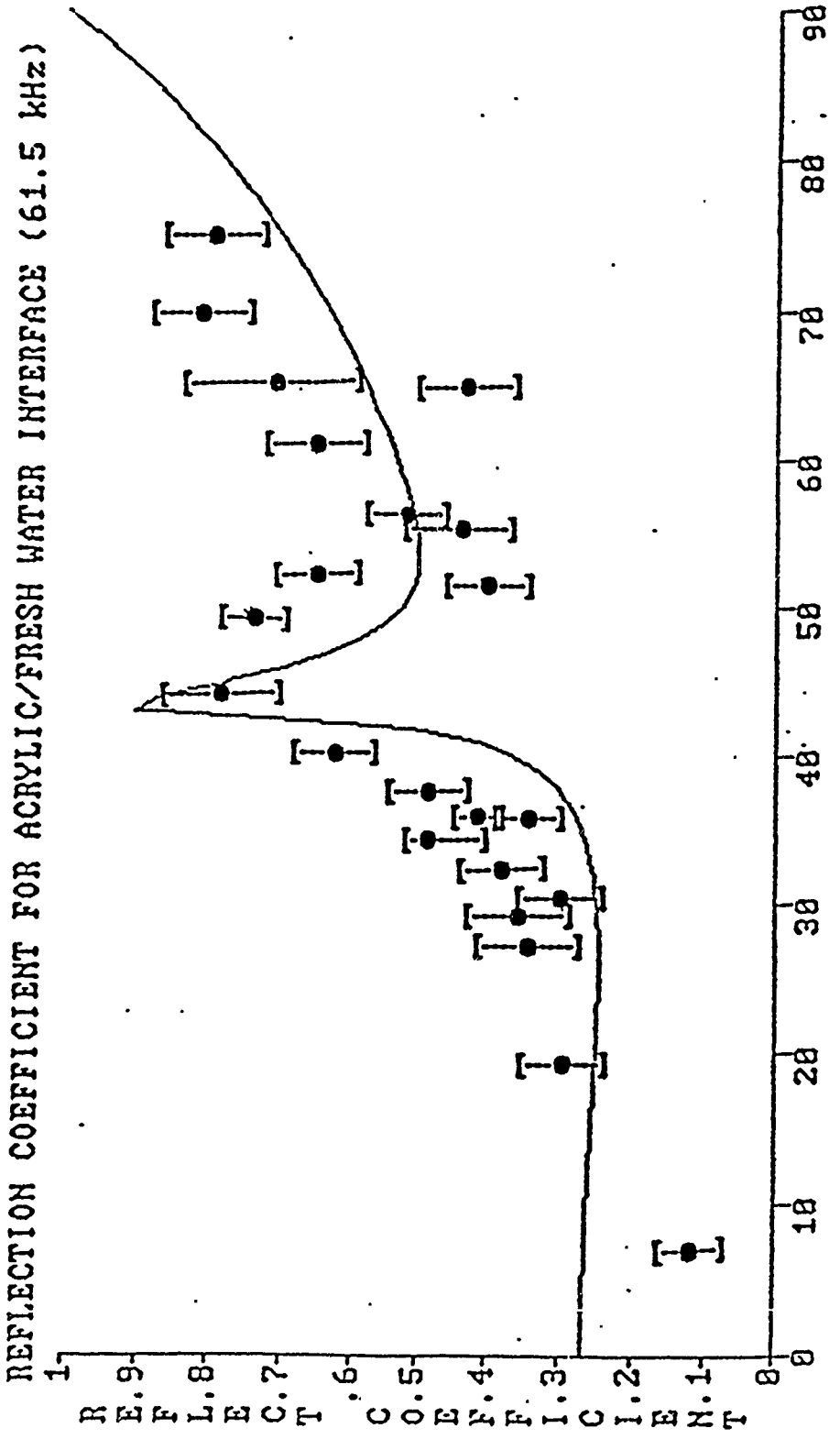

Figure 19(b). The line represents the values of equation (7) plotted with appropriate attenuation factors. The points are experimentally determined mean values with the "error bars" denoting high and low values. This graph is for 61.52 kHz with $\alpha = .18$ and $\beta = 92$.

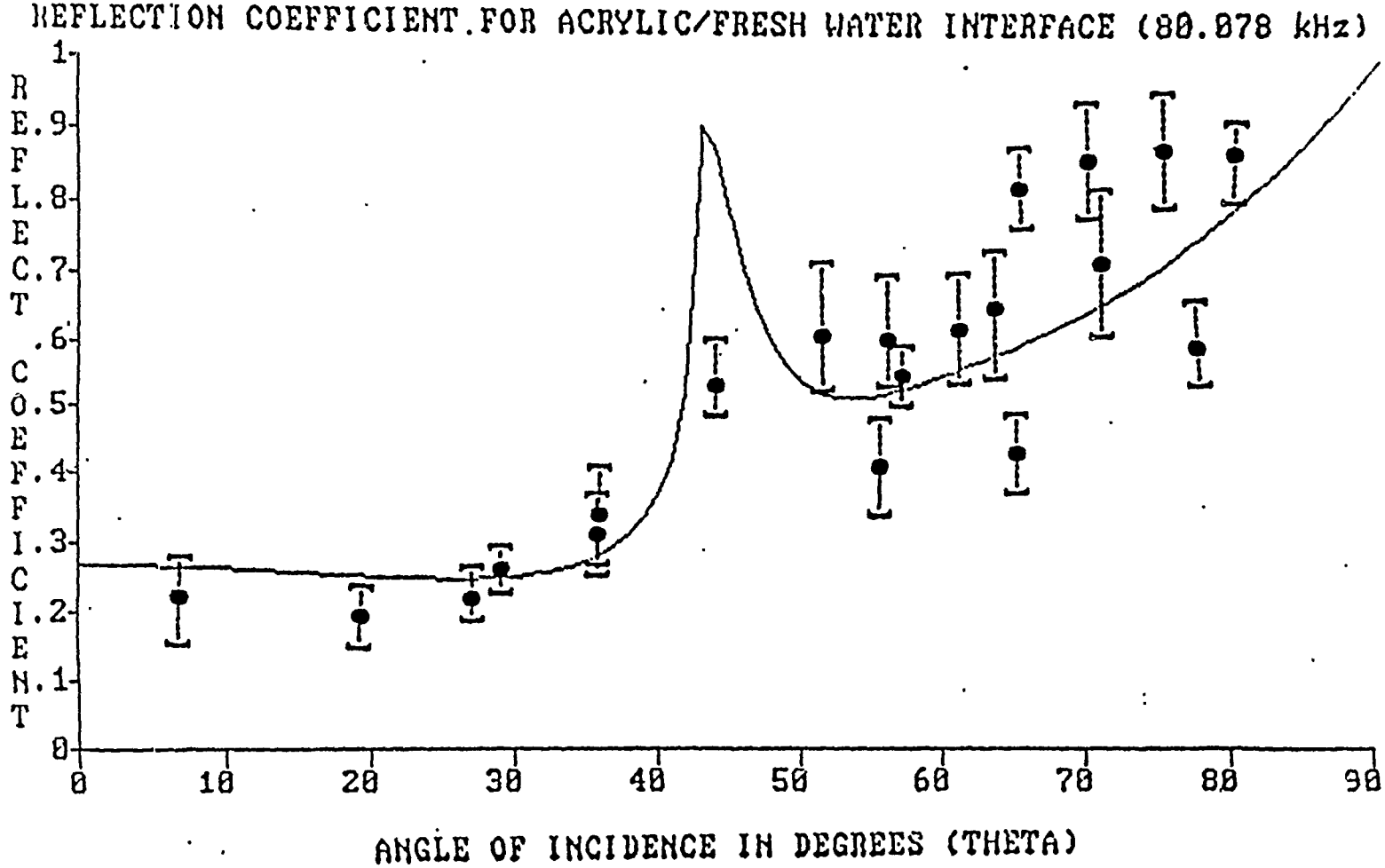

Figure 19(c). The line represents the values of equation (7) plotted with appropriate attenuation factors. The points are experimentally determined mean values with the "error bars" denoting high and low values. This graph is for 80.08 kHz.with $\alpha = .24$ and $\beta = 120$.

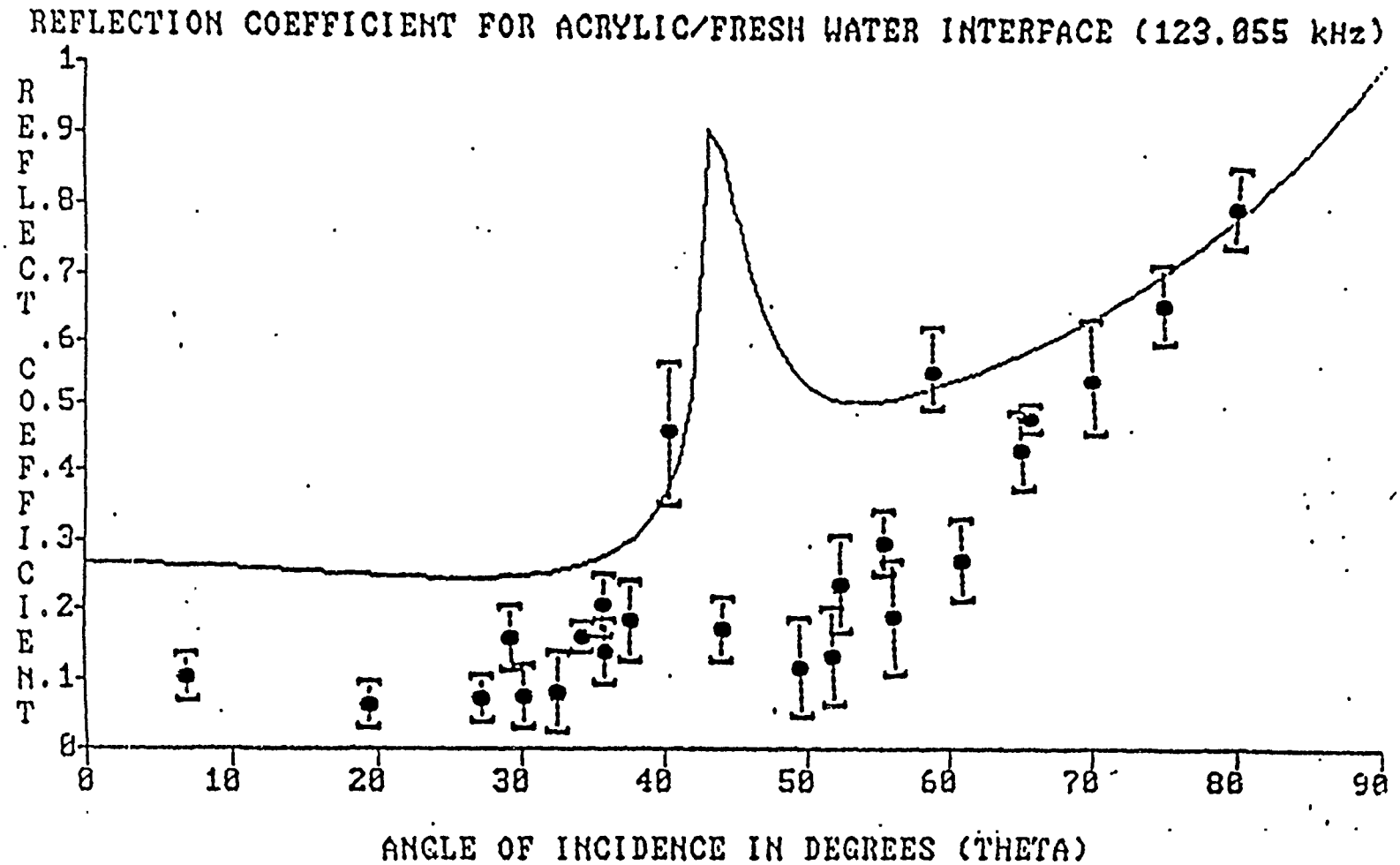

Figure 19(d). The line represents the values of equation (7) plotted with appropriate attenuation factors. The points are experimentally determined mean values with the "error bars" denoting high and low values. This graph is for 123.06 kHz with $\alpha = .37$ and $\beta = 185$.

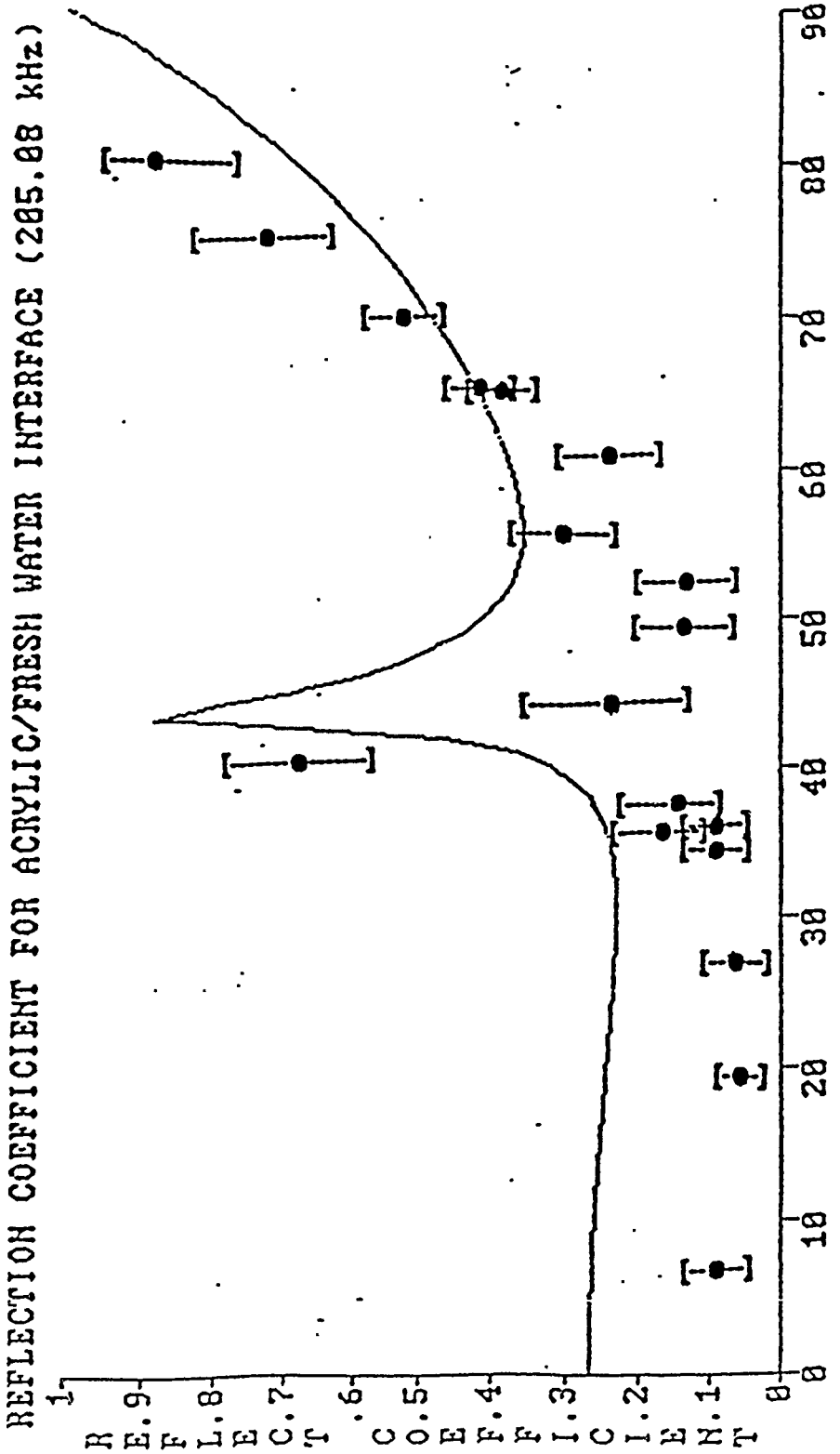

Figure 19(e). The line represents the values of equation (7) plotted with appropriate attenuation factors. The points are experimentally determined mean values with the "error bars" denoting high and low values. This graph is for 205.08 kHz with α = .62 and β = 308.

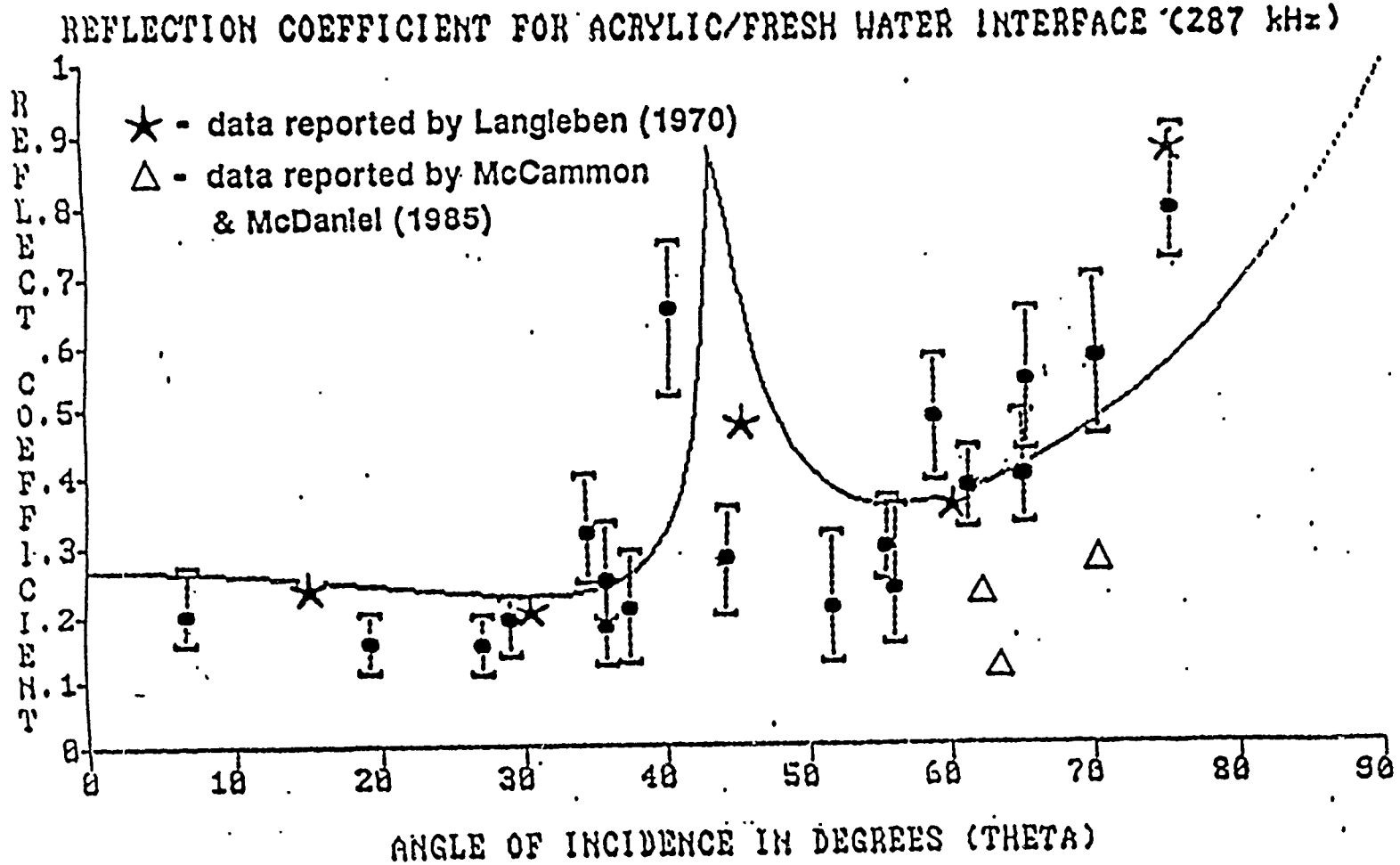

Figure 19(f). The line represents the values of equation (7) plotted with appropriate attenuation factors. The points are experimentally determined mean values with the "error bars" denoting high and low values. This graph is for 287 kHz with $\alpha = .86$ and $\beta = 431$. The triangles represent data reported by McCammon and McDaniel (1985) and the stars data from Langleben (1970).

experimentally derived data points superimposed for each of the six frequencies of interest. A strong correlation is noted between the theoretical and experimental values. The "error bars" denote the high and low experimental values and the range within which the values fell, with the circle denoting the average value.

α was determined to be .003f and β was found to be equal to 1.5f (both with f in kHz and units of $(m\ kHz)^{-1}$) in the laboratory acrylic, using a variety of coefficients to obtain a best fit. These values differ from those reported by others. Denny and Johnson present {.424f and .853f} in dB/m with f also frequency in kHz, and Browne the same for their acrylic. McCammon and McDaniel present $\{.06f(-6/T)^{2/3}$ and $.36f(-6/T)^{2/3}\}$ also in dB/m when T is temperature in °C, for Arctic ice.

The values of reflection coefficients (both the theoretical and laboratory data) correspond closely with the real world data reported by Langleben (1970) and McCammon and McDaniel (1985). The literature reported Arctic data has been plotted on the 287 kHz graph as this is the frequency that is most appropriate given the known scaling parameters. Langleben's 17.9 kHz would be represented by 6.93 MHz in the laboratory model (and is represented by stars on the graphs) and McCammon and McDaniel's 625 Hz corresponds to 276.8 kHz (and is depicted by triangles).

Poor correlation exists between Brekhovskikh's theory with the addition of attenuation effects and the data from all experiments. The fact that experiment and theory do not agree is corroborated by Diachok and Mayer (1969). They note additionally, that losses in reflectivity may be caused by conversion to a Rayleigh-type wave where reflection is conical in nature rather than totally reflected. This would account for poor agreement at angles near θ_{crit}.

Finally there is undoubtedly some error in the collected data as any temperature variations were not accounted for and McCammon and McDaniel define attenuation as temperature dependent. Further, chemical impurities existing in the water also result in alteration of acoustic response. Rust, fiberglass and simple dust accumulation could have altered the water properties sufficiently to disturb the experiment. Despite this, there is strong agreement between experimental data, the Clay and Medwin theoretical plot when their equation is altered to account for attenuation losses, and scaled reported data, particularly that of Langleben.

V. ACOUSTIC SCATTERING

A. THEORETICAL FOUNDATIONS

To begin the study of scattering phenomena Huygen's principle is once again invoked. Treating each distinct parcel of the ensonified object as a re-radiating point source and summing the wave fronts gives an excellent visual model of the scattering process. The effect in this instance, due to the roughness of the object, is energy loss in a variety of directions. The energy of a signal that is normally incident will no longer be reflected exclusively back at the source (Figure 20). Thus, the value of the scattering coefficient will be a function of a myriad of variables, among which are several distinct angles (incidence, object orientation or aspect, direction of interest for scattered wave amplitude) as well as some form of representation of the amount of surface roughness present. This experiment is concerned with that portion of the incident energy which is scattered in the original direction of propagation and thus continues its travel; this is termed forwardscatter.

B. ADDITIONAL ENVIRONMENTAL PARAMETERS OF IMPORT

Several additional parameters become important to consider when expanding the simple, smooth, plane surface Arctic model to include large-scale roughness factors.

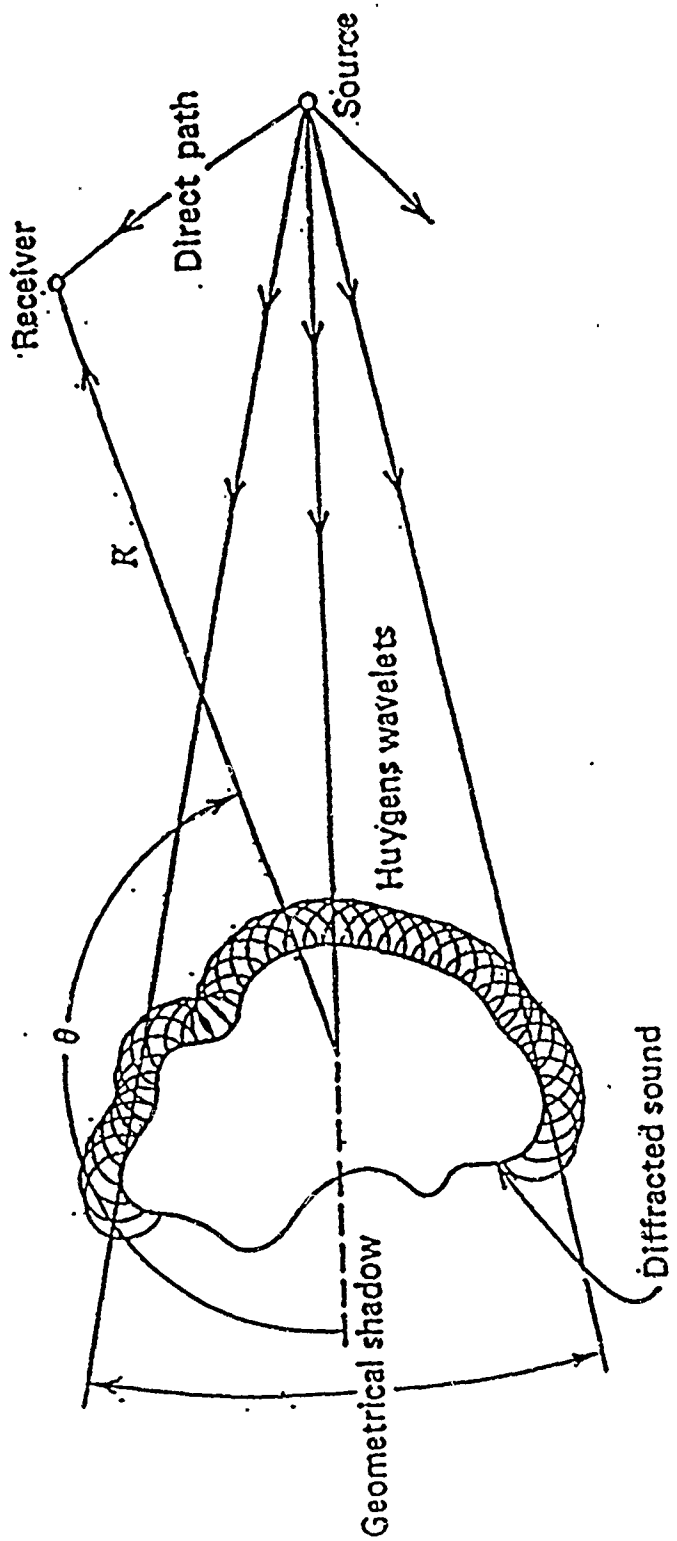

Figure 20. Huygen's principle when applied to the scattering phenomena on a rough-surfaced object. (Clay and Medwin, 1977)

The most obvious of these variables is pressure-ridge keel depth (h), the probability density of which may be modeled by:

$$(2abh + ac)\ e^{-(abh^2 + ach)}$$

where a = the proportionality constant, b = A/h^2, A = cross-sectional area, h = keel depth, $c = \pi\ h/8\ \Omega\ R_o$, Ω = mean keel spacing, R_o = 1.6 or half-width-to-depth ratio (Greene, 1984).

Ridge orientation is another key factor that must be considered. Although it is commonly assumed, for the purposes of modeling, that ridges are directionally isotropic, statistical analyses indicate that in certain regions there may exist a preferred direction for keel orientation (Greene, 1984). The relative probability that a given ridge link of length L will cross the path of concern, is proportional to the length of the projection in the direction perpendicular to the track, L sin(θ), where θ is the angle between the axis of the ridge and the track. The probability density for the angle of intersection of ridges crossing the track is:

$$(1/2)\ \sin(\theta)\ d\theta, \quad \text{for } 0 \leq \vartheta < \pi$$

with the associated distribution function:

$(1/2)\ (1 - \cos(\theta))$ (Greene, 1984).

The "apparent width" of the ridge is a function of the aspect from which the object is viewed. The apparent width is defined as:

$$W_a = W / \sin \theta$$

where θ is the angle of intersection between the axis of the structure and the measurement track. W_a will have a distribution of:

$$\sqrt{(1 - (W/W_a)^2} \quad \text{on } [W,\infty]$$

and a density given by:

$$W^2/(W_a^2 \sqrt{(W_a^2 - W^2)})\ dW_a.$$

Lead edges add further scattering surfaces. In Wadhams (1981) the number density of leads per kilometer of observed width d meters was found to obey a power law:

$$n(d) = 15\ d^{-2}$$

where a lead was defined to be a continuous sequence of depth points, greater than 5 meters long and not exceeding

1 meter of draft, as observed from the perspective of an upward-looking sonar. Greene (1984) states that the density for actual lead width is in fact:

$$p(W) = (1/W_o)\ e^{-W/W_o}.$$

Coherent scattering loss formulae and scattering loss kernels for the incoherent field based on statistical techniques require the autocorrelation for input. In order to calculate the autocorrelation for a rigid surface, one may employ discrete ridge statistics and a specified ridge shape or ensemble of ridge shapes.

C. THEORIES OF SCATTER EFFECTS

The amount of scattering that occurs to the energy incident on an object is partially a function of the wavelength of the waves in question; it is a frequency-related response. Due to this phenomenon the nature in which an object's roughness is described is related to the wavelength of the incident energy. One model of the relative measure of an object's roughness is the Rayleigh parameter (R) which is defined as:

$$R = k * H * \sin(\theta) \qquad \text{(Urick,1983)}$$

where k is the wave number ($2\pi f/c$), H is the root mean

square (rms) "roughness height" and θ is the grazing angle of the impinging acoustic wave. For values of $R << 1$ the surface is defined as a reflector (i.e. it is "acoustically" smooth); and when $R >> 1$ the object is a scatterer (i.e. rough). Thus, an acoustic wave interacts with an object as rough or smooth relative to its own wavelength.

An amplitude reflection coefficient for an irregular surface is defined by Urick (1983) as:

$$\mu = \exp(-R)$$

when R is the Rayleigh parameter as defined as above. Thus, the amount of energy forwardscattered will decrease with increasing frequency or grazing angle (the complement to the incident angle) for any given object. This fact is noted by Denny and Johnson (1986) and Brekhovskikh (1982). Gordon and Bucker (1984) confirm that scattered energy decreases with increasing frequency and increasing roughness. Greene demonstrates increased scattering losses as a function of increased range and frequency.

Brekhovskikh derives an equation for the amount of energy scattered in the forward direction, which he denotes "coherent reflection in the specular direction". He begins with the energy conservation law as applied to the energy of the incident waves. This generates:

$$R = 1 - 2 * k * \cos(\theta o) \int_{\Upsilon_1} G(x) [k^2 - (\varepsilon_o + x)^2]^{1/2} \, dx$$

where k is the specific wave number, θo is the specific angle of incidence, G is the Fourier transform of the correlation function, $x = \{x \cos(\alpha), x \sin(\alpha)\}$ and is the Fourier representation of the wave number when α is the azimuth angle, ε_o is the horizontal component of the wave vector, and Υ_1 defines the region over which the integral is to be taken - in this instance the range is defined for x as 0 to ∞ and for α as $-\pi$ to π. Through algebraic and integrational simplification when applied to the situation of large scale roughness (such as that present in the Arctic) this becomes:

$$R = 1 - R^2/2$$

where R is the Rayleigh parameter as previously defined (Brekhovskikh, 1982).

The Science Applications International Corporation (SAIC) has developed a scaling model for the Arctic environment, termed the SAIC Interim Scattering Model for Ice or SISM/ICE. The standard deviation of roughness is the only parameter that the model requires for predictions. It is valid for acoustic waves with frequencies from 0 to 5000 Hz and grazing angles of 0 to 45 degrees. The under-ice surface is considered to be

flat with the pressure-ridge keels modeled as cylindrical bosses of elliptical cross-section. The following assumptions regarding the bosses are made:

1) they have a half-width-to-depth ratio (R_o) of 1.6
2) they have a Rayleigh depth distribution
3) they have a random orientation
4) they exhibit random spacing along a track

Under-ice roughness spectra measured along a track may be approximated by a two-parameter spectral model. The standard deviation of roughness (σ) derived from such a spectrum is:

$$\sigma^2 = 2c/\beta^2$$

where β is the regression coefficient for the population (Greene, 1984).

The SISM/ICE model is a hybrid of scattering theories based upon both continuous and discrete roughness models. Mean ridge spacing (Ω) is assumed to be 100 m for the purposes of this model. All angles θ are grazing angles. Four formulae are given. The predicted value of R is the maximum of the four calculated values.

Low Frequency-Free Surface Formula

$$R = (1 - 4 \sin(\theta)\ k^2\ \sigma^2\ (1-\pi^2\ c\ \sin(\theta)/2))^{1/2}$$

High Frequency-Free Surface Formula

$$R = (1 - 4 \sin(\theta)\ (1.198)\ c\ (k/\beta)^{3/2})^{1/2}$$

High Frequency-Rigid Surface Formula

$$R = ([\sin(\theta) - x]^2 + x^2)/([\sin(\theta) + x]^2 + x^2) \qquad x < \sin(\theta)$$

$$(.2)^{1/2} \qquad x > \sin(\theta)$$

where $x = 1.311\ c\ (k/\beta)^{1/2}$

Asymptotic Twersky Formula

$$R = [\sin(\theta) - x]/[\sin(\theta) + x]$$

where $x = n\ L \cos(\theta-\tau)$ $\qquad \tan(\tau) = p^{-2} \tan(\theta)$

$L^2 = w^2(\tan^2(\theta) + p^4)/(\tan^2(\theta) + p^2)$

$w = R_o\ \pi\ h/2$ $\qquad p = 2/(R_o\pi)$ $\qquad n = 1/\Omega$ (Greene,1984).

D. FORWARDSCATTER DATA AND CONCLUSIONS

The majority of studies consulted are concerned with backscatter data, as this is the portion of the acoustic energy budget which negatively affects the operation of an active sonar. Reverberation masks the sonar's ability to detect the desired echo signals and is caused by backscatter towards the source. However, this experiment studies the reflection and forwardscatter suitable for long-range propagation effects. Thus, the ability to compare the experimentally determined forwardscatter data

with that from other models and studies was somewhat limited.

Denny and Johnson (1986) report data collected from three grazing angles at fourteen different frequencies ranging from 31.3 to 82 kHz. Their data correspond to 39.1 to 102.5 kHz when scaled to fit the parameters of this experiment. Their mean values of scattering loss per bounce are presented on Figure 21 and shows the expected frequency and angular dependence.

The SISM/ICE model reports theoretical transmission loss as a function of range and compares that to real world data (Figure 22). Similar reliance is again exhibited upon frequency in both their theoretical and experimental data.

Gordon and Bucker (1984) present environmentally obtained data in terms of scattering loss per bounce in Figure 23, which is the same format as Denny and Johnson. The same angular and frequency variation is evident in their data and consistent with theory. Gordon and Bucker's Arctic frequencies correspond to frequencies of 39.7 and 79.4 kHz in the laboratory.

This experiment determined a scattering ratio, defined as the ratio of forwardscattered peak pressure amplitude to direct path peak pressure ampitude. The manner of collection followed was as outlined in the Procedure chapter, for five angles of incidence at six

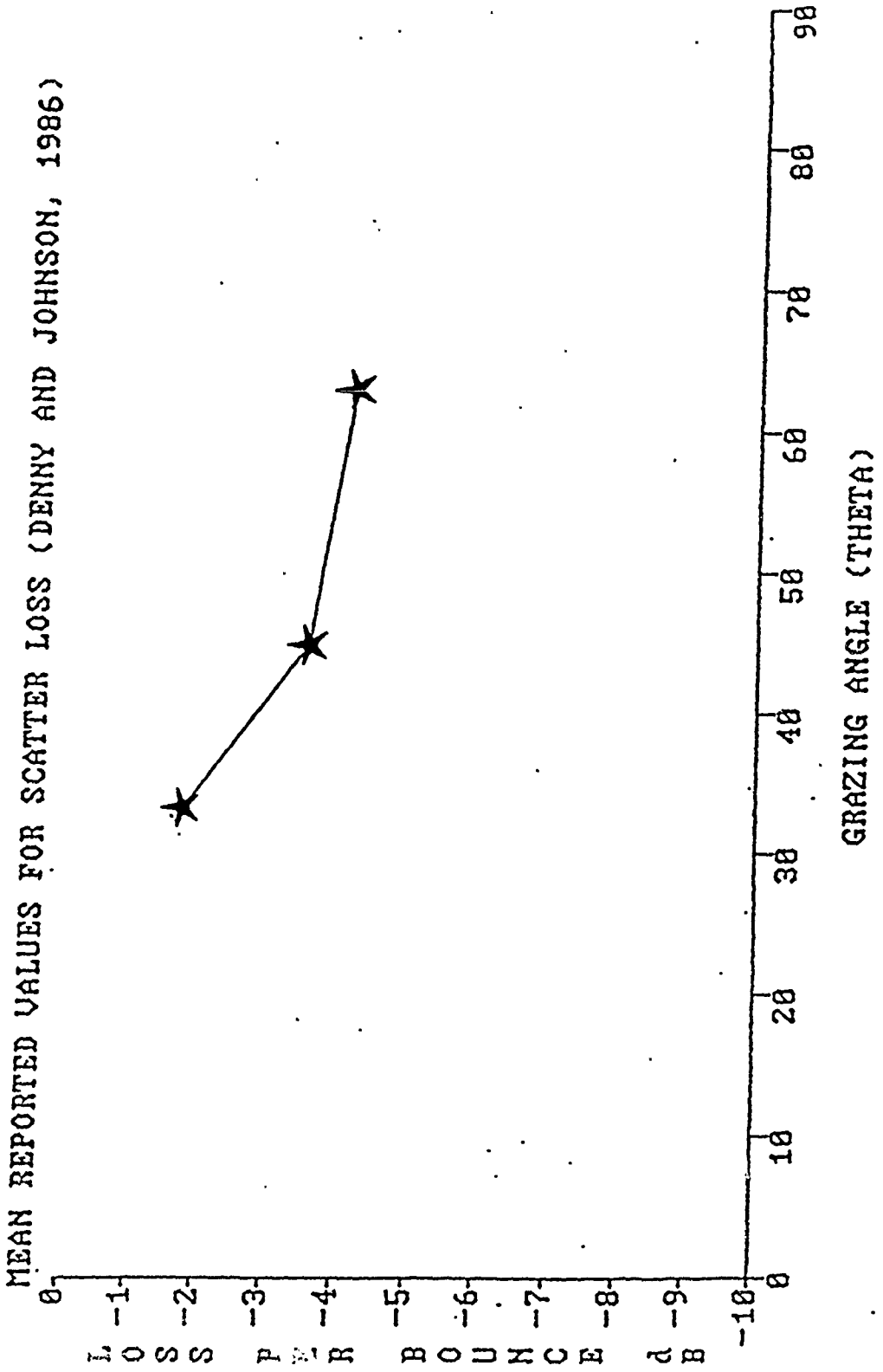

Figure 21. Mean values of scattering loss per bounce as reported by Denny and Johnson (1986)

Environmental and Theoretical Transmission Loss Data for a Rough Surface

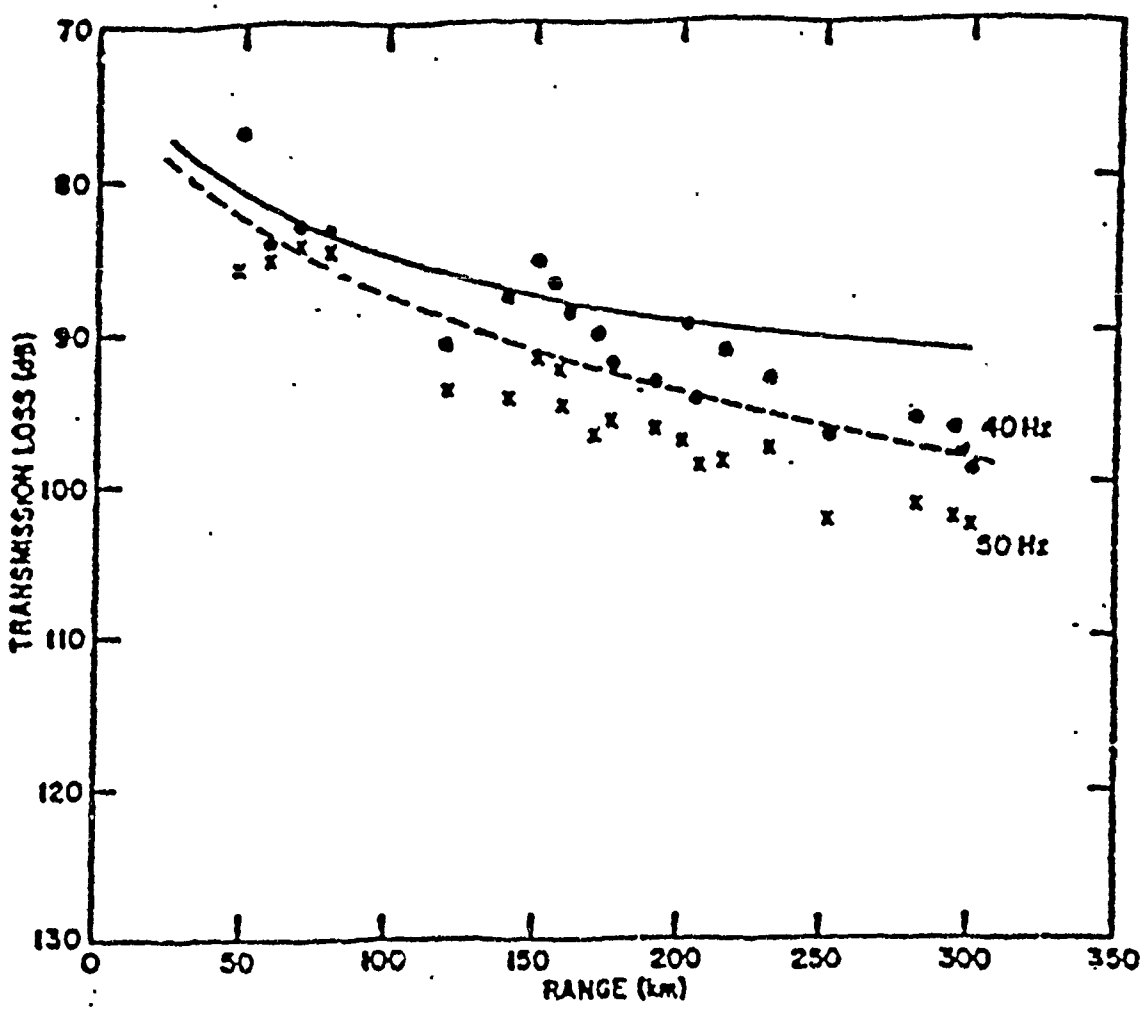

Figure 22. A plot based on a simulated ice surface consisting of equal depth, equally spaced trapezoidal ice keels, transmission-loss data from a Central Arctic site at 40 Hz (....) and 50 Hz (xxxx) compared with simulated transmission-loss at 40 Hz (____) and 50 Hz (----), using the Arctic High Angle Parabolic Equation. (Greene, 1984)

Environmentally Collected Reflection Loss Data

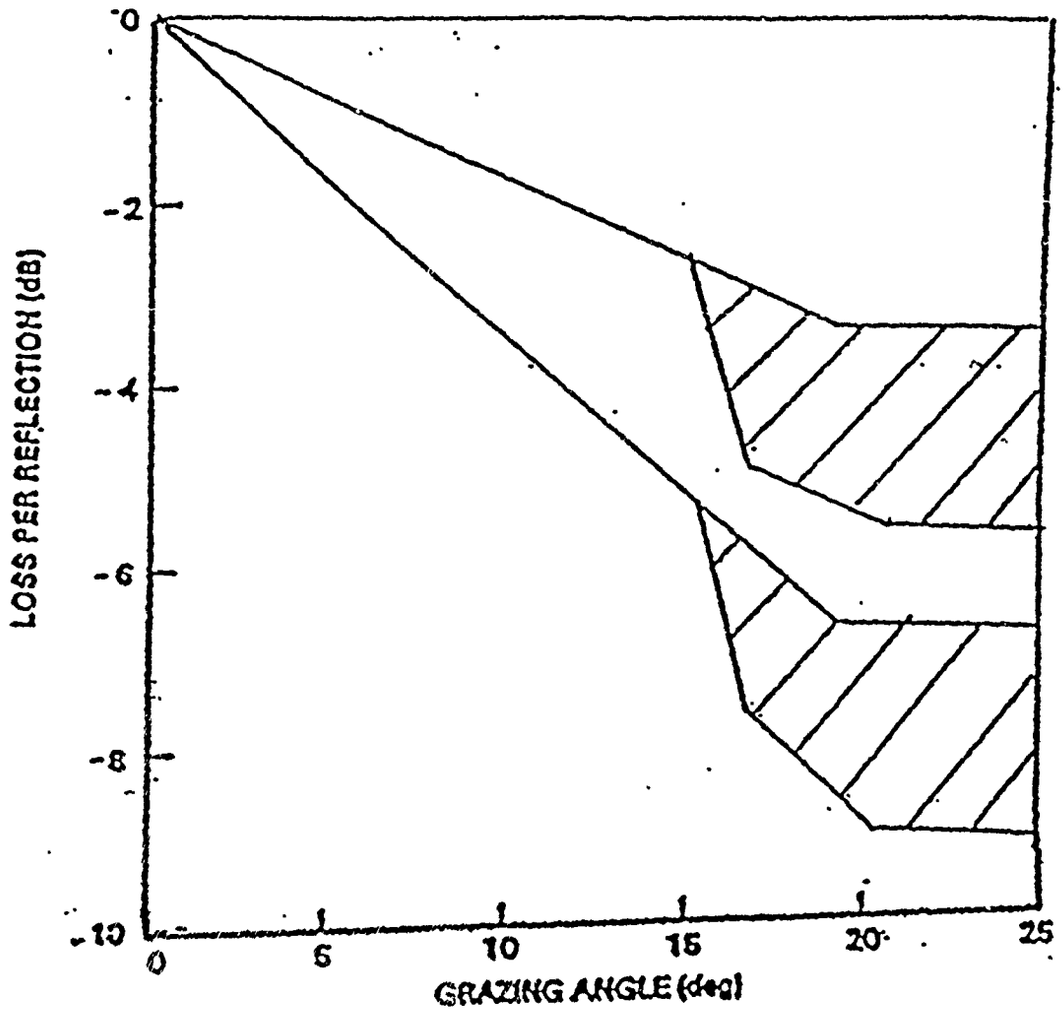

Figure 23. Ice reflection losses as a function of grazing angle at two frequencies as used in the Arctic propagation program. The losses are due to scattering except that part over the shaded area, which is due to ice loss (Gordon and Bucker, 1984)

separate frequencies. This data are plotted in terms of deciBels (dB) on Figure 24 and responds as anticipated. There is some lack of agreement in the extremely high frequency range; at these frequencies large-scale scattering effects occur due to the increased relative size of the keel. Birch (1972) mentions what may have been an additional problem: at frequencies when the surface is "acoustically rough" (i.e. high frequencies), the exact angle of impingement is uncertain, thus prediction of scatter strengths as a function of grazing angle is difficult.

Further, data in this experiment as well as that of Denny and Johnson were collected solely for one "statistically correct" keel, rather than an environmentally correct ridge field as in Greene's reported data. The Gordon and Bucker data are derived from a field of keels but analyzes only one bounce or reflection. This may account for the fact that the losses are up to 40 dB greater for Greene's reported data as compared to the other experimental values of both the laboratory and environment.

Some of the data disparity may also be accounted for by a return to the Rayleigh parameter. For those frequencies chosen in this experiment and an rms roughness height for the keel of .0163 m, the following conclusions are obtained:

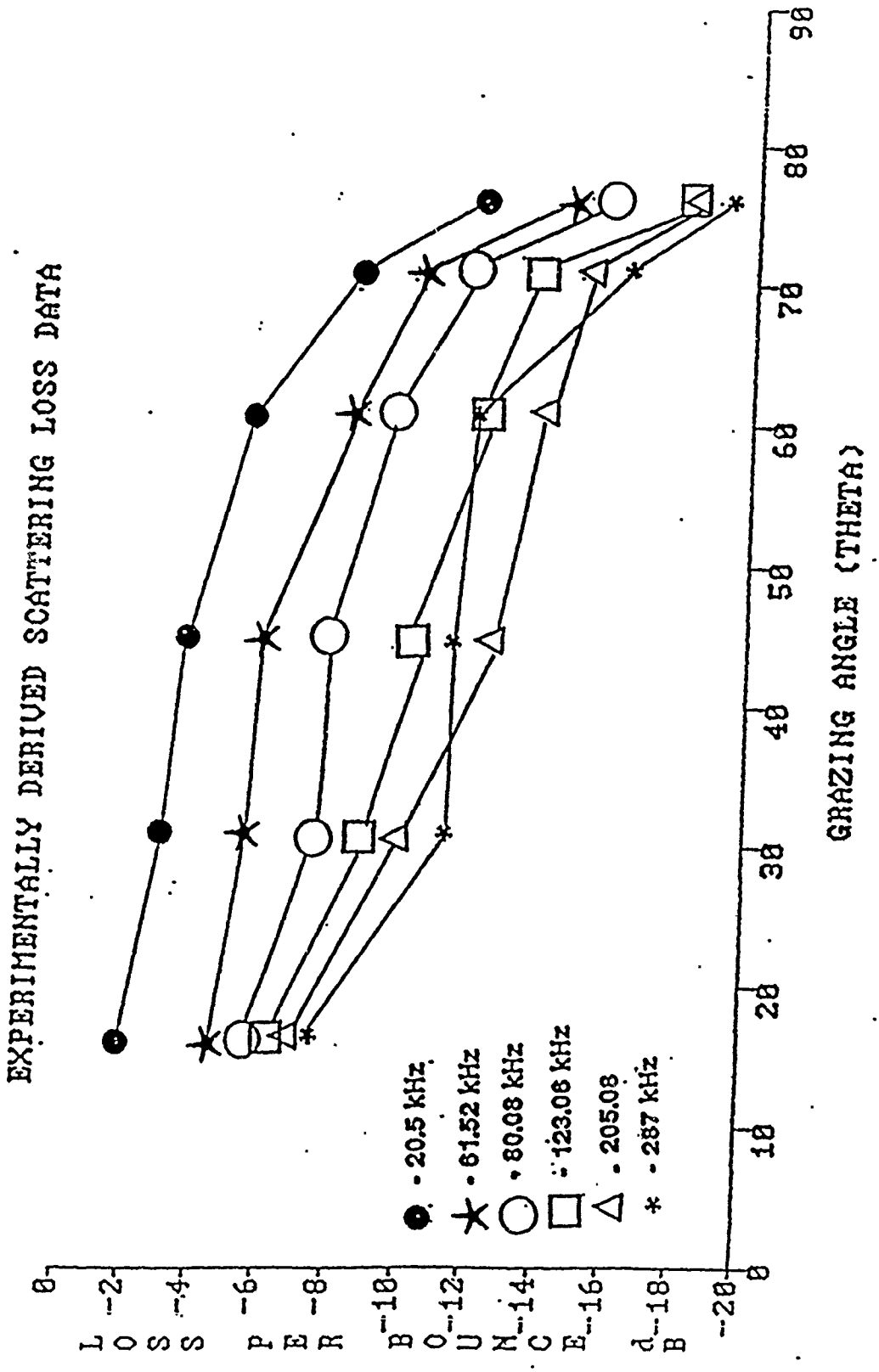

Figure 24. Experimentally derived data for scattering loss per bounce

20.50 kHz	demonstrates smooth surface effects
61.52 kHz 80.08 kHz 123.06 kHz	are in the undefined region, not acoustically smooth or rough
205.08 kHz 287.00 kHz	demonstrates rough surface effects

Thus, the fact that the 20.50 kHz data follows closely that of the reflection data and does not demonstrate large-scale losses is expected. Likewise, the 61.52, 80.08, and 123.06 kHz data fall within the region defined by Rayleigh as exhibiting properties of both. The 205 and 287 kHz are the only frequencies that actually fall within the Rayleigh parameter for roughness for the majority of the angles involved in the experiment. There exists a strong qualitative correlation of frequency and grazing angle dependence between theory and all data. Finally, when comparing this experiment with Denny and Johnson, and Gordon and Bucker (which share similar analysis techniques), quantitative values for scaled frequencies are extremely close.

VI. SUMMARY OF FINDINGS

This paper has presented a series of experiments that modeled the acoustic-ice interactions using burst transmissions from omnidirectional underwater point sources. Floating acrylic plates were employed to represent the Arctic ice due to the similiarity in impedance characteristics and other physical properties to known ice values. Geometrical properties of the ice were accurately scaled in the acrylic by maintaining the appropriate wavelength ratios. Reflection and forwardscatter effects were analyzed and compared with existing theories for the Arctic. Six frequencies were utilized to gather data for both reflection and scattering effects.

The equation presented by Clay and Medwin (1977) for reflection at a liquid-solid interface was modified by the addition of attenuation factors through the use of complex sound speeds. A strong correlation between the revised theoretical and obtained experimental values of the reflection coefficient was noted.

Compressional wave speed attenuation (α) in the .0063 m sheet of Plaskolite™ acrylic utilized in this project was determined to be .003f (f in kHz) and a shear attenuation (β) was found to be equal to 1.5f (f in kHz) with units of $(m\ kHz)^{-1}$. These values differ from those of

others. Denny and Johnson report .424f and .835f in dB/m (f in kHz) for their acrylic, Browne {same} and McCammon and McDaniel $\{.06f(-6/T)^{2/3}$ and $.36f(-6/T)^{2/3}\}$ dB/km kHz for ice.

The values of reflection coefficients (both the theoretical and laboratory data) correspond closely with the real world data reported by Langleben (1970) and McCammon and McDaniel (1985) when scaled to the frequencies appropriate to this experiment.

Poor correlation exists between Brekhovskikh's theory (with or without the addition of attenuation effects) and the data from all experiments. The fact that experiment and theory do not agree is noted by Diachok and Mayer (1969). They have noted additionally that losses in reflectivity may be caused by conversion to a Rayleigh-type wave where reflection is conical in nature rather than totally reflected. This would account for poor agreement at angles near θ_{crit}.

Additionally, there is undoubtedly some error in the data collected, as variations in temperature were not accounted for and McCammon and McDaniel define attenuation with a temperature dependence. Further, chemical impurities existing in the water, such as dust, debris and rust that had entered the tank, could also result in alteration of acoustic response. Despite this, there is strong agreement between experimental data, the Clay and

Medwin theoretical plot when the equation has been altered to account for attenuation losses, and scaled reported data.

Strong frequency and grazing angle dependence was noted in the scattering data, as anticipated. There is some lack of agreement in the higher frequency range; at these frequencies large scale scattering effects occur due to the increased relative size of the keel. Further, data was collected solely for one "statistically correct" keel, rather than an environmentally correct ridge field. Good agreement exists both qualitatively and quantitatively between the values for this experiment, Denny and Johnson's experimental values, and Gordon and Bucker's environmental data.

Further study is required into the acoustic interaction in the colloidal region; research into its modeling will prove beneficial to future understanding. Additional attempts to improve Brekhovskikh's environmentally correct three-medium mathematical model to better fit Arctic data and thereby generate a means of more accurately predicting reflection response will prove extremely important. Investigation of acoustic attenuation in various media will supplement the overall comprehension of reflection and transmission phenomena as well. Continued collection of real world information is also necessary to expand the database and provide insight into

the specific governing factors of the acoustic propagation phenomenon. The Arctic remains a region of complex acoustic interactions and it is only through continued diligent study that it will be possible to successfully conquer this scientific frontier.

REFERENCES

Ackley, S. F. et al., 1976, "Thickness and Roughness Variations Of Arctic Multiyear Sea Ice", Cold Regions Research and Engineering Laboratory Report 76-18, Table II.

Birch, W.B., 1972, "Arctic Acoustics in ASW", IEEE International Conference on Engineering in the Ocean Environment Record, Institute of Electrical and Electronic Engineers, Inc., NY, NY, p. 293-297.

Brekhovskikh, L. and Yu. Lysanov, 1982, Fundamentals of Ocean Acoustics, Springer-Verlag.

Brekhovskikh, L., 1980, Waves in Layered Media, Academic Press, Inc.

Browne, M. J., 1987, "Underwater Acoustic Backscatter from a model of Arctic Ice Open Leads and Pressure Ridges", Naval Postgraduate School, Monterey, CA.

Bunney, R. E., 1974, "Feasibility of acoustically determining the thickness of sea ice", Applied Physics Laboratory, University of Washington.

Clay, C. S. and H. Medwin, 1977, Acoustical Oceanography: Principles and Applications, Wiley & Sons.

Covault, C., "Soviet Ability to Fire Through Ice Creates New SLBM Basing Mode," Aviation Week and Space Technology, December 10, 1984, pp. 16-17.

Denny, P. L., and K. R. Johnson, 1986, "Underwater Acoustic Scatter from a Model of the Arctic Ice Canopy," Naval Postgraduate School, Monterey, CA.

Diachok, O. I., and W. G. Mayer, 1969, "Conical Reflection of Ultrasound from a Liquid-Solid Interface," J. Acoust. Soc. Am., 47 (1), pp. 155-157.

Diachok, O. I., 1974, Naval Oceanographic Office Technical Note No. 6130-4-74, Effects of Sea Ice Ridge Characteristics on Under-Ice Reflection Loss in Arctic/Subarctic Waters, p. 11.

Francois, R. E., and T. Wen, 1983, "Use of Acoustics in Localizing Under-Ice Oil Spills", Applied Physics Laboratory, University of Washington.

Frank, W. H., 1988, Introduction to TK Solver Plus, Universal Technical Systems, Inc., Rockford, Illinois.

Gere, J. M. and S. P. Timoshenko, 1984, Mechanics of Materials, Wadsworth, Inc.

Gordon, D. F. and H. P. Bucker, 1984, "Arctic Acoustic Propagation Model with Ice Scattering", Naval Oceans Systems Center.

Greene, R. R., 1984, Ice Statistics and Acoustic Scattering in the Arctic Basin, Science International Corporation (SAIC-84-1132) for Naval Ocean Research and Development Activity, p. 1-1 to 1-5.

Hibler, W. D. III, W. F. Weeks, and S. J. Mock, 1974, "Statistical Aspects Of Sea-Ice Ridge Distributions," J. Geo. Rsch., 79, pp. 2735-2743.

Hobbs, P. V. Ice Physics. Clarendon Press, Oxford, 1974.

Kleinerman, M. M., 1980, "Naval Concerns in the Seasonal Sea Ice Zone", Naval Surface Weapons Center.

Langleben, M. P., 1970, "Reflection of Sound at the Water-Sea Ice Interface," J. Geo. Rsch, 75 (27), pp. 5243-5246.

McCammon, D. F. and S. T. McDaniel, 1985, "The influence of the physical properties of ice on reflectivity," J. Acoust. Soc. Am., 77 (2), pp. 499-507.

Medwin, H., M. J. Browne, K. R. Johnson, and P. L. Denny, 1988, "Low-frequency backscatter from Arctic leads," J. Acoust. Soc. Am., 83 (5), pp. 1794-1803.

Mellen, R. H., P. M. Scheifele, and D. G. Browning, 1987, Global Model for Sound Absorption in Seawater Part III: Arctic Regions, Naval Underwater Systems Center, Newport RI: NUSC Technical Report 1969, p. 1-29.

Meyers, J. J., C. H. Holme, and R. F. McAllister, eds., Handbook of Ocean and Underwater Engineering, pp. 1-8, McGraw-Hill Book Co.

Plaskolite Technical Information Sheet, Plaskolite, Inc., Columbus, Ohio.

Shwartz, J., and W. F. Weeks, 1977, "Engineering Properties of Sea Ice", J. Glac., 19, pp. 499-531.

Urick, R. J., 1983, Principles of Underwater Sound, McGraw-Hill, Inc.

Vidmar, P. J., 1987, "Synopsis of an Investigation of the Acoustic Properties of Sea Ice", Applied Research Laboratories, University of Texas at Austin.

Wadhams, P., 1981, "Sea-ice topography of the Arctic Ocean in the region 70°W to 25°E", Philosophical Transactions of the Royal Society of London, 302, 45-85.

Weeks, W. F., A. Kovacs, and W. D. Hibler III, 1976, "Pressure Ridge Characteristics In The Arctic Coastal Environment," Proceedings from the First International Conference on Port and Ocean Engineering under Arctic Conditions, I, pp. 152-183.

Welsh, J. P., R. D. Ketchum Jr., A. W. Lohanick, L. D. Farmer, D. T. Eppler, R. E. Burge, and C. J. Radl, 1986, A compendium of Arctic Environmental Information, Naval Ocean Research and Development Activity, Report 138, p. 28-35.

APPENDIX

There were two primary computational obstacles at the outset of the experiment. The first was separating the desired return signal from the myriad of extraneous echoes. These undesired reflections would occur due to the confines of the relatively small tank within which operation of the model occurred. Rather than employ a filtering or gating system which might distort the return data, it was decided that the desired pulse would be manually (i.e. visually) extracted from the return. In order for this to be performed it was necessary to calculate a "window" within which the reflected pulse could be anticipated. Further, knowledge of the time that the other reflected pulses would be arriving would serve to help elucidate the "signal" from the "noise", or more accurately, the one desired reflection from those not desired.

The second problem was a lack of data on the particular acoustic parameters governing the acrylic sheet. The specifications provided by the acrylic manufacturers were obviously not acoustic in nature. It was thus necessary to apply the known data with the aid of several equations to determine the characteristics of the acrylic and describe the model in a more appropriately acoustical fashion.

The Universal Technical Systems, Inc. TK Solver Plus™ equation processor software was employed to solve these problems. It utilizes a declarative or rule-based programming language that permits direct input of a series of equations and subsequent analysis of the effects of either single or multiple variable manipulation. "TK" stands for "tool kit" and is an excellent description of the utility of the software (Frank 1988).

Specifically in this experiment, the parameters of hydrophone placement and tank dimensions were entered. Through the use of a simple array of trigonometric equations the angles, distances, and time windows of interest were calculated. The software saved numerous hours of hand computation of these values. Additionally, the use of this technique enabled the data to be collected free from filtering or gating devices as time separation of the incident pulse from the various reflections was ensured. This allowed for a "purer", less technically or electronically distorted signal and therefore more accurate data and conclusions.

Limited data were available regarding the acrylic parameters for the laboratory. Seeking theoretical values with which to compare those determined experimentally, the following derivational method was employed. Given a specific gravity from the Plaskolite™ Properties Sheet and taking a value of water density of 998.84 kilograms/cubic

meter (kg/m^3), the density of acrylic was determined to be 1189.8 kg/m^3. The sheet also provided a bulk modulus of elasticity of 449,000 pounds per square inch. Conversion of this value to mks units resulted in 3.097×10^9 Newtons/m^2. The technical information available however extended no further. Employing the TK Solver Plus™ program, which allows for iterative analyses, the remainder of the acrylic parameters were determined theoretically. This employed the following four equations and the two known values to solve for the four unknown parameters:

σ (sigma) - Poisson's Ratio E - bulk modulus of elasticity

G - bulk modulus of rigidity p - density of acrylic

c - compressional wave speed in acrylic c_s - shear wave speed in acrylic

$$\sigma = [3E - p * c^2]/[3E + p * c^2] \quad a$$

$$c^2 = [E + 4/3 * G]/ p \quad a$$

$$E = 2 * (1 + \sigma) * G \quad b$$

$$c_s^2 = G/p \quad a$$

This provided the following values:

c = 1939.0273 meters/second	c_s = 931.47804 m/s
σ = .5000258	G = 1.03233 X 10^9 N/m^2
E = 3.097 X 10^9 N/m^2	p = 1189.8 kg/m^3

a - (Clay and Medwin, 1977)

b - (Gere, 1984)